

Stochastic phase-field modeling of brittle fracture: computing multiple crack patterns and their probabilities

Tymofiy Gerasimov¹, Ulrich Römer², Jaroslav Vondřejc³,
Hermann G. Matthies³, and Laura De Lorenzis⁴

¹Institut für Angewandte Mechanik,
Technische Universität Braunschweig, Germany

²Institut für Dynamik und Schwingungen,
Technische Universität Braunschweig, Germany

³Institute of Scientific Computing,
Technische Universität Braunschweig, Germany

⁴Department of Mechanical and Process Engineering,
ETH Zürich, Switzerland

5th May 2020

Abstract

In variational phase-field modeling of brittle fracture, the functional to be minimized is not convex, so that the necessary stationarity conditions of the functional may admit multiple solutions. The solution obtained in an actual computation is typically one out of several local minimizers. Evidence of multiple solutions induced by small perturbations of numerical or physical parameters was occasionally recorded but not explicitly investigated in the literature. In this work, we focus on this issue and advocate a paradigm shift, away from the search for one particular solution towards the simultaneous description of all possible solutions (local minimizers), along with the probabilities of their occurrence. Inspired by recent approaches advocating measure-valued solutions (Young measures as well as their generalization to statistical solutions) and their numerical approximations in fluid mechanics, we propose the stochastic relaxation of the variational brittle fracture problem through random perturbations of the functional. We introduce the concept of *stochastic solution*, with the main advantage that point-to-point correlations of the crack phase fields in the underlying domain can be captured. These stochastic solutions are represented by random fields or random variables with values in the classical deterministic solution

spaces. In the numerical experiments, we use a simple Monte Carlo approach to compute approximations to such stochastic solutions. The final result of the computation is not a single crack pattern, but rather several possible crack patterns and their probabilities. The stochastic solution framework using evolving random fields allows additionally the interesting possibility of conditioning the probabilities of further crack paths on intermediate crack patterns.

Keywords: brittle fracture, phase-field model, multiple solutions, random perturbation, stochastic solution, Young measure

Contents

1	Introduction	3
2	Deterministic modeling	7
2.1	Phase-field formulation of brittle fracture	7
2.2	Model example: anti-plane shear test	10
2.3	Numerical results	13
3	Stochastic modeling: some informal examples	15
3.1	Minimization of a double-well function	15
3.2	Fracture of a 1D bar with a sharp crack approach	17
3.3	Fracture of a 1D bar in the phase-field setting	20
4	Stochastic phase-field modeling of brittle fracture	23
4.1	Preliminaries	23
4.1.1	Random variables and random fields	23
4.1.2	Random phase fields	24
4.1.3	Quantities of interest	25
4.1.4	Separated representation	25
4.1.5	Random displacement fields	26
4.1.6	Stochastic constraints	27
4.2	Stochastic formulation of the variational problem	27
4.3	Some remarks about Young measures	29
4.4	Numerical computations	30
4.4.1	Random perturbations	30
4.4.2	Computing statistical moments	31
4.4.3	Computing crack pattern probabilities	34
5	Conclusions	36

1 Introduction

The phase-field approach to brittle fracture dates back to the seminal work of Francfort and Marigo [1] on the variational formulation of quasi-static brittle fracture and to the related regularized variational formulation of Bourdin et al. [2, 3, 4, 5]. The former is the mathematical theory of quasi-static brittle fracture mechanics, which recasts Griffith’s energy-based principle as the minimisation problem of an energy functional. The latter presents an approximation, in the sense of Γ -convergence, of this energy functional and enables an efficient numerical treatment.

The phase-field formulation of fracture holds a number of advantages over the classical techniques based on a discrete fracture description, whose numerical implementation requires explicit (in the classical finite element method) or implicit (within e.g. the extended finite element method) handling of the discontinuities. The most obvious one is the ability to track automatically a cracking process with arbitrarily complex crack topology, featuring e.g. coalescence and branching, also in three dimensions, by describing the evolution of a smooth *crack phase field (which can be interpreted as a damage field)* on a fixed mesh. Another advantage is the ability to describe crack nucleation, also in the absence of singularities, without the need for ad-hoc criteria. Also, by adopting a formulation capable to distinguish between fracture behavior in tension and compression, no supplementary contact problem has to be posed for preventing crack faces interpenetration. For these reasons, phase-field formulations of brittle fracture have attracted a lot of attention in the past decade, see e.g. [6, 7, 8, 9, 10, 11, 12, 13, 14, 15, 16, 17, 18, 19, 20, 21, 22, 23]. Although several extensions to more complex material behavior and coupled formulations with additional fields (e.g. temperature, concentration etc.) have been proposed, in this work we focus our attention on quasi-static brittle fracture.

As typical for solid mechanics problems in presence of softening behavior [65, 66], the functional to be minimized is non-convex with respect to its two arguments (displacement field and crack phase field) simultaneously. This implies that the governing equations of the coupled problem, which are obtained as the necessary conditions of stationarity of the functional with respect to the two arguments, may admit multiple solutions. Since no general numerical algorithm exists which can guarantee global minimization for a non-convex problem, the solution obtained in the computational practice is typically a local minimizer¹. The occurrence of multiple solutions has been occasionally reported in the literature, e.g. in [2, 3, 5, 8, 27, 29, 30]. Some of the examples are illustrated in Figure 1.

Figure 1(a) depicts the results obtained in [5] for the traction test on a fiber-reinforced matrix in plane stress. A square elastic matrix is bonded to a rigid circular fiber. The fiber is fixed, while a uniform vertical displacement is applied to the upper edge of the matrix, and the remaining sides are traction free. The computations are performed on an unstructured triangular uniform finite element mesh using the alternate minimization solution

¹Note that the solutions may even correspond to local maxima or saddle points, which can only be clarified by a stability analysis. The questions as to what critical point we actually compute [3] and to which type of minimizer (global or local) represents a physically meaningful solution [4] remain beyond the scope of this paper.

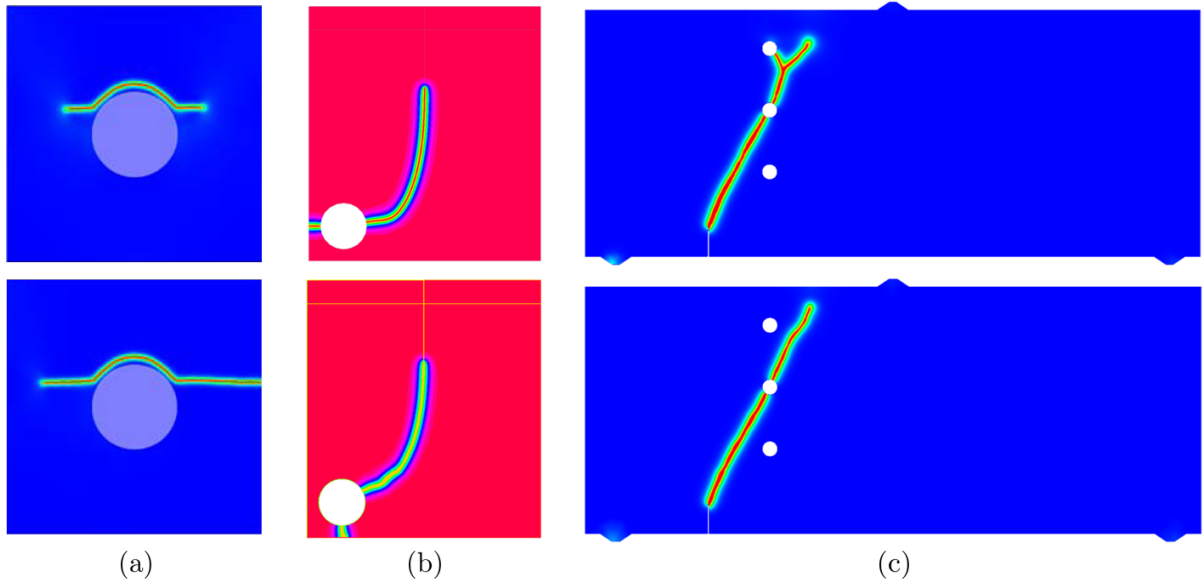


Figure 1: Examples of non-unique solutions (in terms of crack path): the fiber-reinforced matrix traction test [5] (similar findings in [2, 3, 8]), (b) the anti-plane shear test [30] (also in [27, 29]), (c) the notched three-point bending test from [36].

algorithm. In the beginning stage of the monotonically increasing loading, a crack nucleates and propagates symmetrically with respect to the vertical axis. However, subsequently the solution loses symmetry and the authors comment that an asymmetric solution “is consistent with the lack of uniqueness of the solution for the variational formulation”.

Figure 1(b) reports two solutions of the anti-plane shear experiment considered in [30]. The setup, which we also adopt in our numerical experiments in this paper, is detailed in section 2.2. In [30], two solution algorithms are proposed, which differ in the sequence of alternate minimization and mesh adaptivity: Algorithm 1 (*solve-then-adapt*) applies mesh adaptation after the convergence of the minimization procedure, whereas with Algorithm 2 (*solve-and-adapt*) mesh adaptivity is carried out at each minimization iteration. The results leading to the top and bottom plots in Figure 1(b) are obtained using Algorithm 2 with anisotropic and isotropic adaptive triangulation, respectively.

Finally, Figure 1(c) presents our findings for the notched three-point bending experiment originally designed in [36] with the aim of studying the effect of structural imperfections such as holes on crack trajectories. Our computations performed for one of the setups in [36] lead to two different solutions. In both cases, the same triangular finite element mesh is used, which is pre-adapted in the region where crack propagation is expected, but we use different increments of the applied displacement. The results shown correspond to the last loading step, featuring in both cases the same magnitude of applied displacement.

The above results suggest the following *numerical* factors as possible triggers of multiple solutions:

- finite element mesh, including e.g. the choice of fixed vs. adaptive, isotropic vs. anisotropic mesh,
- solution algorithm, e.g. hierarchy of multiple nested iterative solution processes or choice of the tangent stiffness matrix in monolithic solution schemes [25, 26],
- parameters related to the solution algorithm (loading increments, thresholds, tolerances, termination criteria, etc.),
- round-off errors.

On the other hand, small perturbations of *physical* parameters (geometry parameters or material properties, i.e. elastic moduli or fracture toughness) may also lead to multiple solutions. As opposed to the perturbation of numerical parameters, the latter can be interpreted as representing physically meaningful variations in the geometry and material properties which would also be encountered in reality (e.g. in experiments).

Despite the above findings, to the best of the authors’ knowledge, no attempt has been made so far to intentionally investigate and characterize the encountered multiple solutions.

In the present work, we aim at addressing the issue of solution non-uniqueness for phase-field modeling of brittle fracture. In doing so we advocate a paradigm shift, from the search for one solution to the simultaneous description of *all* possible solutions (local minimizers) along with the probabilities of their occurrence.

To this end, we shift from a deterministic to a stochastic formulation, so that the multiple deterministic solutions appear as possibilities of a probabilistic solution, where the different probabilities reflect the energy landscape which may favour one possibility over another one. This stochastic formulation may be viewed as a relaxation of the original variational problem. Note that the concept of relaxation is not uncommon for non-convex problems. As follows, we outline some of the available approaches.

One relaxation approach builds on parameterized measures (Young measures and their generalizations), which are able to describe oscillatory or concentration effects of minimizing sequences [43, 44, 50] in minimization problems. They are mainly used as a tool for relaxation (generalization) of mathematical formulations which lack minimizers [45]. As examples one can name damage evolution in elastic materials [74], micromagnetics and shape memory alloys [46, 47], optimal control [48, 49], or fluids [50]. A recent inspiring approach focuses on measure-valued solutions and their numerical approximations for systems of hyperbolic conservation laws [38, 40, 42, 39, 41] in the context of fluid mechanics. In these papers, the field problem is reformulated with Young measure-valued solutions and extended to what is called a “statistical solution” — an infinite system of Young correlation measures — which defines a probability measure on a function space, building on a solution concept which goes back at least to Foias, cf. [75] for a concise account. This is in fact a special case of a more general construct which has been variously termed a “weak distribution” or “operational process” [76, 77, 78], resp. a “generalised stochastic process” [79] — a construction which seems to be more suited to infinite dimensional Hilbert and Banach spaces than the stricter concept of a probability measure, and one which

is inherently connected with a weak or variational problem formulation. This extension or relaxation of the solution space is used in [42, 38] to show that in this extended sense there is a unique solution to certain systems of hyperbolic conservation laws. In [38, 40] a Monte Carlo method is used for these systems of hyperbolic conservation laws to sample the solution as a random variable in order to compute its mean and variance field, which then are unique quantities. Due to oscillations of the numerical solution on ever finer grids, such a statistical solution model does not require an underlying uncertainty of physical model parameters, although they can be integrated seamlessly. In the case of brittle fracture which is of interest here, such oscillations do not occur as meshes are refined, it is rather the possible alternative crack paths we want to capture, and some stochastic perturbation will be introduced.

Beside the inspiration by this idea of statistical solutions, the work we report in this paper also uses methods from similar work for stochastic problems in mechanics and applied sciences, where a formulation based on spectral approximations in a Galerkin setting was proposed in [54], and then extended in a variational framework to linear elasticity [55, 56], covering also theoretical aspects. This was further extended to a variational theory also for nonlinear problems [57], as well as to thermodynamically irreversible and highly non-smooth problems of infinitesimal plasticity [58, 59] — which is in many ways close to the present case of quasi-brittle fracture — within the framework of convex analysis [60]. In plasticity, uniqueness of the solution can only be established in the presence of hardening, and is lost when one considers perfect plasticity.

In this paper we pursue a relaxation of the variational problem of phase-field regularized brittle fracture by allowing the solution to be a random variable with values in the deterministic solution space, i.e. a *stochastic solution*. The randomness is introduced through some small random perturbation in the energy functional, which becomes itself a random variable. The idea is to minimise the *expected value* of the energy functional over an appropriate space of random fields, and then look at the limiting behaviour of the stochastic solution as the random perturbation becomes smaller and smaller.

Thus we try to capture all non-unique solutions in a stochastic solution. Compared to a formulation based on Young measures, such an approach results in solutions which are random fields, and allows to capture point-to-point correlations of the crack phase fields in the underlying domain. This seems also to be at least as general as the idea of a structure of Young correlation measures in [42, 38]. The difference is that we work with random fields or abstract random variables with values in the deterministic space of possible solution fields, rather than probability measures. Just as in e.g. [56, 57, 60], this has certain advantages, as these abstract random variables or random fields live freely in vector spaces, whereas probability measures are constrained by the requirements of being positive and necessarily integrating to one, i.e. they lie on the intersection of the positive quadrant (or cone) with the unit ball in some appropriate measure space. Although the resulting sets of such probability measures are convex, the mentioned constraints usually require particular care when discretisations and numerical approximations have to be used in the actual computation of an approximate solution. Formulations in terms of abstract random variables or random fields on the other hand look completely analogous to the usual

deterministic variational formulations, and thus allow for the use of the deterministic solver codes; no new equations have to be formulated and new solver programs to be developed and implemented for probabilistic descriptors like higher moments [75], or systems of Young correlation measures [42, 38] for statistical solutions. An important question was whether by this kind of relaxation it would be possible to achieve a unique albeit probabilistic solution, as in [56, 57, 60]. As shown in Section 3, it seems that uniqueness is by no means automatic through such a relaxation, and there seems to be a dependence of the stochastic solution on the kind of perturbation. Thus it becomes natural to expect that random perturbations be connected with the ones actually occurring in the physical systems being modelled. For a given type of perturbation, with the proposed approach the final result of the computation is not a crack pattern (along with the corresponding global and local results, e.g. load-displacement curve, displacement field, etc.), but rather several possible crack patterns (with the additional associated results) as well as their probabilities. Such results have obviously a much higher computational cost, however, they also have a much higher information content.

The paper is organised as follows. In Section 2 we outline the main concepts of phase-field modeling of brittle fracture and the formulation used in the present paper. We adopt the numerical setup in Figure 1(b) taken from [30], and in addition to the two crack patterns obtained in the original reference we find a third one by computing on fixed meshes. We term these results deterministic and use them as a motivation and a starting point for the following developments. The stochastic analysis is introduced in Section 3 in a simple one-dimensional setting, first based on Griffith's theory and then formulated for phase-field modeling. In Section 4 we present the proposed stochastic approach in a rather general setting and apply it to the anti-plane shear case study of Section 2. Finally, conclusions are drawn in Section 5.

2 Deterministic modeling

In this section, we briefly recall the main concepts of the phase-field framework for modeling brittle fracture, and then introduce the anti-plane shear test as reference example. For this test we capture three different fracture mechanisms by perturbing the finite element mesh and the loading increment. We also present energy-displacement curves to enable preliminary considerations on the energetic equivalence of the multiple solutions obtained.

2.1 Phase-field formulation of brittle fracture

Let $D \subset \mathbb{R}^m$ ($m = 2$ or 3) be an open and bounded domain representing the configuration of a d -dimensional body, and let $\Gamma_{\text{Dir},0}$, $\Gamma_{\text{Dir},1}$ and $\Gamma_{\text{Neum},1}$ be the (non-overlapping) portions of the boundary ∂D of D on which homogeneous Dirichlet, non-homogeneous Dirichlet and Neumann boundary conditions are prescribed, respectively. The material is assumed to be linearly elastic, with the elastic strain energy density function $\Psi(\boldsymbol{\varepsilon})$, where $\boldsymbol{\varepsilon} := \boldsymbol{\varepsilon}(\mathbf{u})$ is the infinitesimal strain, $\boldsymbol{\varepsilon} = \nabla_s \mathbf{u} = \frac{1}{2}(\nabla \mathbf{u} + (\nabla \mathbf{u})^\top)$, and \mathbf{u} is the displacement. In the

isotropic case considered here $\Psi(\boldsymbol{\varepsilon}) = \frac{1}{2}\lambda(\text{tr } \boldsymbol{\varepsilon})^2 + \mu \text{tr } (\boldsymbol{\varepsilon} \cdot \boldsymbol{\varepsilon})$, with λ and μ as the Lamé constants. Also, let G_c be the material fracture toughness or critical energy release rate. We consider a quasi-static loading process with the discrete pseudo-time step parameter $n = 1, 2, \dots$, such that the displacement $\bar{\mathbf{u}}_n$ and traction $\bar{\mathbf{t}}_n$ loading data are prescribed on the corresponding parts of the boundary. Finally, let $\Gamma_c \subset D$ be the crack surface that is evolving during the process, see the left plot in Figure 2.

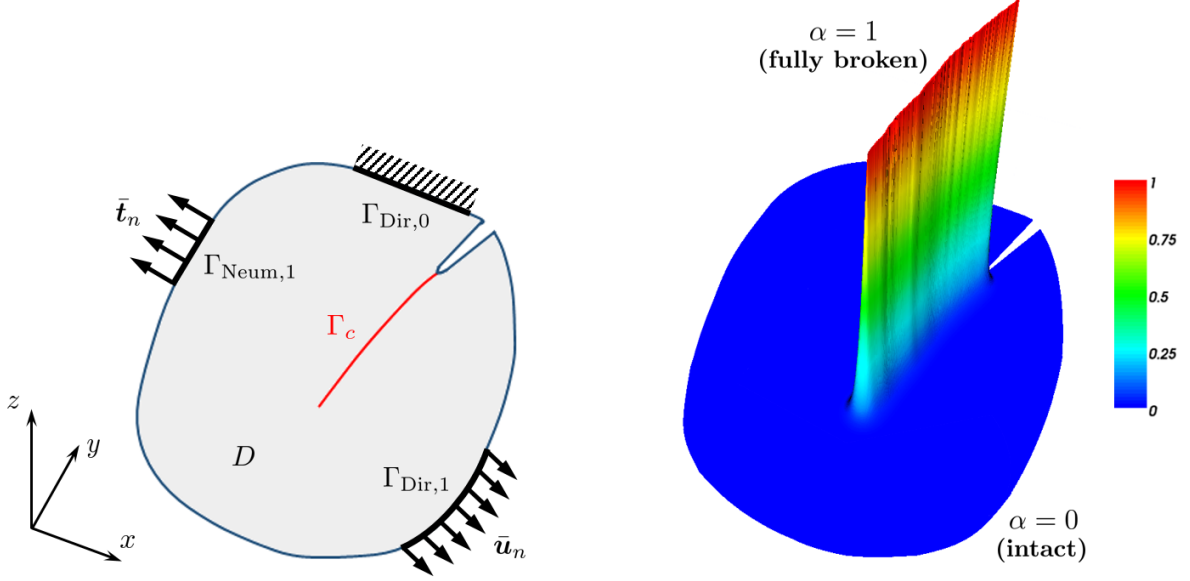


Figure 2: Mechanical system and phase-field description of fracture (sketchy in two dimensions) with $\alpha \in C(D; [0, 1])$ as the crack phase field.

For the mechanical system at hand, the variational approach to brittle fracture in [1] relies on the energy functional

$$E(\mathbf{u}, \Gamma_c) = \int_{D \setminus \Gamma_c} \Psi(\boldsymbol{\varepsilon}(\mathbf{u})) \, d\mathbf{x} + G_c \mathbb{H}^{m-1}(\Gamma_c) - \int_{\Gamma_{\text{Neum},1}} \bar{\mathbf{t}}_n \cdot \mathbf{u} \, ds, \quad (1)$$

and the related minimization problem at each $n \geq 1$. In (1), $\mathbf{u} : D \setminus \Gamma_c \rightarrow \mathbb{R}^d$, $d = 1, 2$, or 3, such that $\mathbf{u} = \mathbf{0}$ on $\Gamma_{\text{Dir},0}$ and $\mathbf{u} = \bar{\mathbf{u}}_n$ on $\Gamma_{\text{Dir},1}$ is the displacement field, $\boldsymbol{\varepsilon} := \boldsymbol{\varepsilon}(\mathbf{u}) : D \setminus \Gamma_c \rightarrow \mathbb{R}^d$ is the strain field Γ_c is the crack set, and \mathbb{H}^p is the so-called p -dimensional Hausdorff measure of Γ_c . The first term in (1) represents the elastic energy stored in the body, and the second one the fracture surface energy dissipated within the fracture process. In simple terms, $\mathbb{H}^1(\Gamma_c)$ and $\mathbb{H}^2(\Gamma_c)$ are the length and the surface area of Γ_c when $d = 2$ and 3, respectively².

²Assuming G_c to be non-constant in D , a more general representation of the fracture energy term in (1) reads $\int_{\Gamma_c} G_c(\mathbf{x}) \mathbb{H}^{m-1}(d\mathbf{x})$, see also Section 4.

The regularization of (1) *à la* Bourdin-Francfort-Marigo [2, 3, 4, 5], which is the basis for a variety of fracture phase-field formulations, reads as follows:

$$E(\mathbf{u}, \alpha) = \int_D g(\alpha) \Psi(\boldsymbol{\varepsilon}(\mathbf{u})) \, d\mathbf{x} + \frac{G_c}{c_w} \int_D \left(\frac{w(\alpha)}{\ell} + \ell |\nabla \alpha|^2 \right) \, d\mathbf{x} - \int_{\Gamma_{\text{Neum},1}} \bar{\mathbf{t}}_n \cdot \mathbf{u} \, ds, \quad (2)$$

with $\mathbf{u} : D \rightarrow \mathbb{R}^d$ and $\alpha : D \rightarrow [0, 1]$ standing for the smeared counterparts of the discontinuous displacement and the crack set in (1). The phase field variable α takes the value 1 on Γ_c , decays smoothly to 0 in a subset of $D \setminus \Gamma_c$ and then vanishes in the rest of the domain, as sketched in the right plot in Figure 2. With this definition, the limits $\alpha = 1$ and $\alpha = 0$ represent the fully broken and the intact (undamaged) material phases, respectively, whereas the intermediate range $\alpha \in (0, 1)$ mimics the transition zone between them. The function g is responsible for the material stiffness degradation. The function w defines the decaying profile of α , whereas the parameter $0 < \ell \ll \text{diam}(D)$ controls the thickness of the localization zone of α , i.e. of the transition zone between the two material states.

The specific choice of the functions g and w in (2) establishes the rigorous link between (1) and (2) when $\ell \rightarrow 0$ via the notion of Γ -convergence, see e.g. Braides [32], Chambolle [33], also giving a meaning to the induced constant c_w . Thus, g is a continuous monotonic function that fulfills the properties: $g(0) = 1$, $g(1) = 0$, $g'(1) = 0$ and $g'(\alpha) < 0$ for $\alpha \in [0, 1)$, see e.g. Pham et al. [13]. The quadratic polynomial $g(\alpha) := (1 - \alpha)^2$ is the simplest choice. The function w , also called the local part of the dissipated fracture energy density function [13], is continuous and monotonic such that $w(0) = 0$, $w(1) = 1$ and $w'(\alpha) \geq 0$ for $\alpha \in [0, 1]$. The constant $c_w := 4 \int_0^1 \sqrt{w(t)} \, dt$ is a normalization constant in the sense of Γ -convergence. The two suitable candidates for w which are widely adopted read $w(\alpha) = \alpha$ and α^2 , such that $c_w = \frac{8}{3}$ and 2, respectively.

The combinations of formulation (2) with the aforementioned choices for g and w are typically termed the AT-1 and AT-2 models, see Table 1. AT stands for *Ambrosio-Tortorelli* and the corresponding type of regularization, see [34]. The main difference between the two models is that AT-1 leads to the existence of an elastic stage before the onset of fracture, whereas using AT-2 the phase-field starts to evolve as soon as the material is loaded, see e.g. [8, 13, 19] for a more detailed explanation. Other representations for g and w are available in the literature, see e.g. [14, 17, 21, 28].

Table 1: *Ingredients of formulation (2).*

g	w	name
$(1 - \alpha)^2$	α	AT-1 model
	α^2	AT-2 model

With E defined by (2), the sought solution at a given loading step $n \geq 1$ is given by

$$(\mathbf{u}, \alpha) = \arg \min \{E(\mathbf{v}, \beta) : \mathbf{v} \in \mathcal{U}_n, \beta \in \mathcal{P}_n\}. \quad (3)$$

Here

$$\mathcal{U}_n := \{\mathbf{u} \in \mathbf{H}^1(D; \mathbb{R}^d) : \mathbf{u} = \mathbf{0} \text{ on } \Gamma_{\text{Dir},0}, \mathbf{u} = \bar{\mathbf{u}}_n \text{ on } \Gamma_{\text{Dir},1}\} \quad (4)$$

is the kinematically admissible affine displacement space satisfying the non-homogeneous Dirichlet condition at load step n with $\mathbf{H}^1(D; \mathbb{R}^d)$ as the usual Sobolev space of functions with values in \mathbb{R}^d , and

$$\mathcal{P}_n := \{\alpha \in \mathcal{P} : \alpha \geq \alpha_{n-1} \text{ in } D\} \subset \mathcal{P} := \mathbf{H}^1(D; \mathbb{R}) \quad (5)$$

is the admissible convex subset for α at time n with α_{n-1} known from the previous loading step in the Sobolev space of phase fields \mathcal{P} . The condition $\alpha \geq \alpha_{n-1}$ in D is used to enforce the *irreversibility* of the crack phase field evolution. It is the backward difference quotient form of $\dot{\alpha} \geq 0$ in D .

The necessary optimality conditions for $(\mathbf{u}, \alpha) \in \mathcal{U}_n \times \mathcal{P}_n$ at every loading step $n \geq 1$ read as follows:

$$\begin{cases} E_{\mathbf{u}}(\mathbf{u}, \alpha; \mathbf{v}) = \langle \delta_{\mathbf{u}} E(\mathbf{u}, \alpha), \mathbf{v} \rangle = 0 \quad \forall \mathbf{v} \in \mathcal{U}, \\ E_{\alpha}(\mathbf{u}, \alpha; \beta - \alpha) = \langle \delta_{\alpha} E(\mathbf{u}, \alpha), \beta - \alpha \rangle \geq 0 \quad \forall \beta \in \mathcal{P}_n, \end{cases} \quad (6)$$

where $E_{\mathbf{u}}$ resp. $\delta_{\mathbf{u}} E$ and E_{α} resp. $\delta_{\alpha} E$ denote the partial Gâteaux derivatives (first variations) of the energetic functional E w.r.t. \mathbf{u} and α , and $\langle \cdot, \cdot \rangle$ is an appropriate duality pairing. The displacement test space in (6) is

$$\mathcal{U} := \mathbf{H}_{\Gamma}^1(D; \mathbb{R}^d) := \{\mathbf{v} \in \mathbf{H}^1(D; \mathbb{R}^d) : \mathbf{v} = \mathbf{0} \text{ on } \Gamma_{\text{Dir},0} \cup \Gamma_{\text{Dir},1}\}, \quad (7)$$

the displacement fields with homogeneous boundary conditions. As noted in the introduction, conditions (6) characterize in general a local minimum of E (or even only a local stationary point).

2.2 Model example: anti-plane shear test

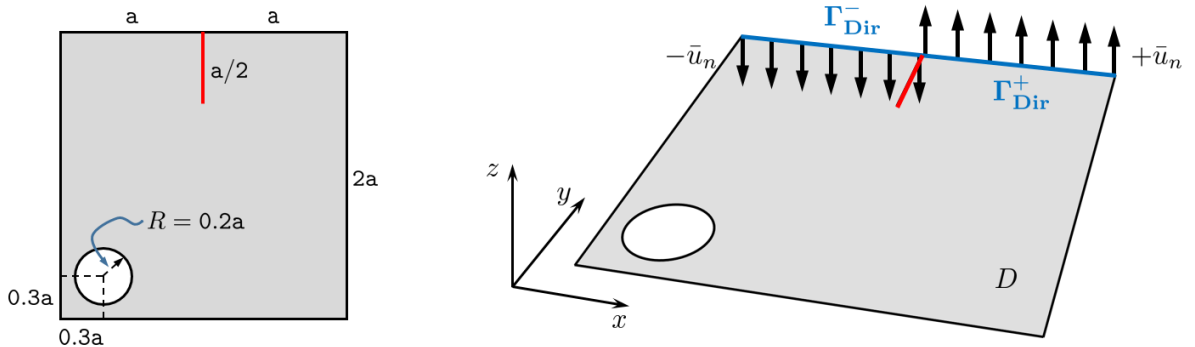


Figure 3: Geometry and loading setup for the anti-plane shear experiment.

Following [30], we consider a two-dimensional rectangular domain $(0, 2\mathbf{a}) \times (0, 2\mathbf{a})$ containing a slit along $\{\mathbf{a}\} \times (3\mathbf{a}/2, 2\mathbf{a})$ and a circular hole with center $(0.3\mathbf{a}, 0.3\mathbf{a})$ of radius $R = 0.2\mathbf{a}$. The incremental anti-plane displacement $\mp \bar{u}_n$, $n \geq 1$ is applied on $\Gamma_{\text{Dir}}^- := (0, \mathbf{a}) \times \{2\mathbf{a}\}$ and $\Gamma_{\text{Dir}}^+ := (\mathbf{a}, 2\mathbf{a}) \times \{2\mathbf{a}\}$, respectively, see Figure 3.

The energy functional used in the incremental minimization problem in this case reads:

$$E(u, \alpha) = \frac{1}{2} \int_D (1 - \alpha)^2 \mu |\nabla u|^2 \, d\mathbf{x} + \frac{G_c}{c_w} \int_D \left(\frac{w(\alpha)}{\ell} + \ell |\nabla \alpha|^2 \right) \, d\mathbf{x} + \frac{\gamma}{2} \int_D \langle \alpha - \alpha_{n-1} \rangle_-^2 \, d\mathbf{x}. \quad (8)$$

The first term in (8) is the corresponding one from the standard formulation in (2) adapted to the anti-plane shear situation: we assume $\mathbf{u} = (0, 0, u_z)$ and $u_z = u : D \subset \mathbb{R}^2 \rightarrow \mathbb{R}$, such that $\boldsymbol{\varepsilon} = \nabla u : D \rightarrow \mathbb{R}^2$ with $\nabla := [\partial x, \partial y]^\top$. The last term is a penalty term which enforces the irreversibility constraint $\alpha \geq \alpha_{n-1}$ via penalization with $\langle y \rangle_- := \min(0, y)$ and $\gamma \in \mathbb{R}_+$ as the penalty parameter, see [31].

Upon the incorporation of the penalty term, the necessary conditions (6) turn into a system of equalities, reading

$$\begin{cases} E_u(u, \alpha; v) = \langle \delta_u E(u, \alpha), v \rangle = 0 & \forall v \in \mathcal{U}, \\ E_\alpha(u, \alpha; \beta) = \langle \delta_\alpha E(u, \alpha), \beta \rangle = 0 & \forall \beta \in \mathcal{P}, \end{cases} \quad (9)$$

where

$$E_u(u, \alpha; v) = \langle \delta_u E(u, \alpha), v \rangle := \int_D (1 - \alpha(\mathbf{x}))^2 \mu \nabla u(\mathbf{x}) \cdot \nabla v(\mathbf{x}) \, d\mathbf{x}, \quad (10)$$

$$\begin{aligned} E_\alpha(u, \alpha; \beta) = \langle \delta_\alpha E(u, \alpha), \beta \rangle &:= - \int_D \mu (1 - \alpha(\mathbf{x})) |\nabla u(\mathbf{x})|^2 \beta(\mathbf{x}) \, d\mathbf{x} \\ &+ \frac{G_c}{c_w} \int_D \left(\frac{1}{\ell} w'(\alpha(\mathbf{x})) \beta(\mathbf{x}) + 2\ell \nabla \alpha(\mathbf{x}) \cdot \nabla \beta(\mathbf{x}) \right) \, d\mathbf{x} \\ &+ \gamma \int_D \langle \alpha(\mathbf{x}) - \alpha_{n-1}(\mathbf{x}) \rangle_- \beta(\mathbf{x}) \, d\mathbf{x}. \end{aligned} \quad (11)$$

The staggered solution algorithm for the system in (9) implies alternately fixing u and α and solving the corresponding equations until convergence. The algorithm is sketched in Table 2. Note that the phase-field evolution equation $E_\alpha = \delta_\alpha E = 0$ is non-linear due to the Macaulay brackets term $\langle \cdot \rangle_-$. Therefore, a Newton-Raphson procedure is used to iteratively compute $\alpha^{(k)}$ with $\alpha^{(k-1)}$ taken as the initial guesses and TOL_{NR} as the tolerance for the corresponding residual.

In the computations, we set $\mathbf{a} = 1$, $\mu = 1$, $\ell = 2\mathbf{a}/50 = 0.04$, $G_c = 1$. In what follows, we choose the quadratic local function $w(\alpha) = \alpha^2$ such that $c_w = 2$. Also, we set $\gamma = \frac{G_c}{\ell} \left(\frac{1}{\text{TOL}_{\text{ir}}^2} - 1 \right)$, where $\text{TOL}_{\text{ir}} = 0.01$. As argued in [31], this choice of γ provides a sufficiently accurate enforcement of $\alpha \geq \alpha_{n-1}$. The applied displacement is given by $\bar{u}_n = n\Delta\bar{u}$, $n = 1, \dots, \frac{3}{2\Delta\bar{u}}$, with $\Delta\bar{u}$ as the loading increment. The deterministic results will be presented for $\Delta\bar{u} \in \{0.01, 0.1\}$ in order to evaluate the impact of the increment size on the ability to trigger solution non-uniqueness. The error tolerances are prescribed as $\text{TOL}_{\text{NR}} := 10^{-6}$ and $\text{TOL}_{\text{Stag}} := 10^{-4}$.

Input: loading data $\pm \bar{u}_n$ on Γ_{Dir}^\pm , and
solution (u_{n-1}, α_{n-1}) from step $n - 1$.

Initialization, $k = 0$:

1. set $(u^{(0)}, \alpha^{(0)}) := (u_{n-1}, \alpha_{n-1})$.

Staggered iteration $k \geq 1$:

2. given $u^{(k-1)}$, solve $E_\alpha(u^{(k-1)}, \alpha; \beta) = 0 \forall \beta$ for α , set $\alpha := \alpha^{(k)}$,
3. given $\alpha^{(k)}$, solve $E_u(u, \alpha^{(k)}; v) = 0 \forall v$ for u , set $u := u^{(k)}$,
4. for the obtained pair $(u^{(k)}, \alpha^{(k)})$, check
 $\text{Res}_{\text{Stag}}^{(k)} := |E_\alpha(u^{(k)}, \alpha^{(k)}; \beta)| \leq \text{TOL}_{\text{Stag}} \forall \beta$,
5. if fulfilled, set $(u^{(k)}, \alpha^{(k)}) := (u_n, \alpha_n)$ and stop;
else $k + 1 \rightarrow k$.

Output: solution (u_n, α_n) .

Table 2: Staggered iterative solution algorithm for (9) at loading step $n \geq 1$.




Crack path type	Type 1	Type 2	Type 3
Crack path (schematically)			

Table 3: Crack paths classification.

In our simulations we employ the numerical package FreeFem++ [35]. Both the displacement field u and the crack phase-field α are approximated using P_1 -triangles. We construct three types of finite element meshes. **Mesh 1** and **Mesh 2** are pre-adapted meshes which are refined in the region of D where crack propagation is expected, see Figure 4. They differ only by the shape of the refined region, but have identical mesh size characteristics (h_{\min}, h_{\max}) . Here, h_{\min} and h_{\max} stand for the mesh size inside and outside of the refined region, respectively. The left plot in Figure 4 depicts the meshes with $(h_{\min}, h_{\max}) := (\frac{1}{4}\ell, \ell)$. Notice that the right plot of the figure aims at illustrating the perturbation character of the considered meshes (that is, one of them can be viewed as a perturbation of the other one), as we assume such perturbation is needed for capturing non-unique solutions. Additionally to **Mesh 1** and **Mesh 2**, we also consider a uniform mesh whose mesh size h is set to h_{\min} used in the corresponding pre-adapted cases. This uniformly fine mesh denoted as **Mesh 3** can be treated as the reference one in the sense of the solution discretization error, as quantities like, e.g. the elastic energy, the fracture energy, as well as the total energy are computed most accurately on this mesh. In the following deterministic computations, we also vary the minimum mesh size h_{\min} , namely, we set $h_{\min} \in \{\frac{1}{4}\ell, \frac{1}{5}\ell, \frac{1}{6}\ell\}$. For a given **Mesh n**, $n = 1, 2, 3$, this can be viewed as another kind of mesh perturbation, and we intend to assess also its effect on the possibility to trigger multiple solutions.

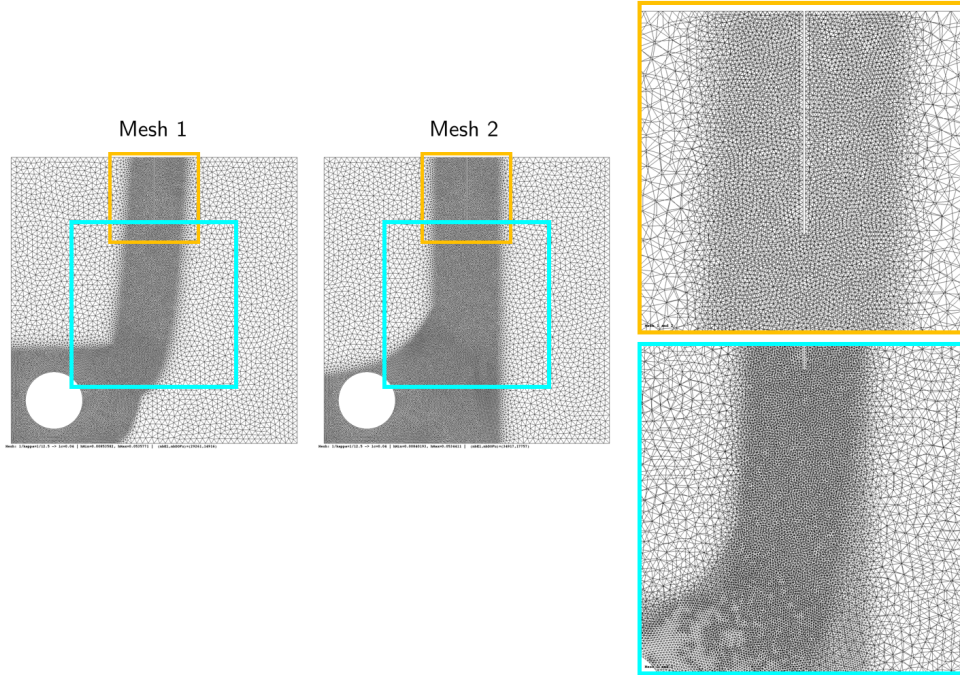


Figure 4: Finite element meshes (on the left) and their overlapping in the marked regions (on the right); the latter is to illustrate that one mesh can be viewed as a perturbation of the other one.

2.3 Numerical results

In Figure 5, the computational results for the three described types of mesh with varying minimum mesh size and for the loading increment $\Delta\bar{u} = 0.01$ are presented. As expected, both the change of the type of mesh and the change of h_{\min} may lead to a change in the final crack pattern. Interestingly, additionally to the two fracture mechanisms reported in [30] (curved crack path which connects the notch and the hole, and then leaves the hole either vertically or horizontally), we also observe a third one which is represented by the (almost) vertical crack that seems attracted by the hole only slightly, yet does not reach it, see the plot for **Mesh 2** with $(h_{\min}, h_{\max}) := (\frac{1}{4}\ell, \ell)$ in Figure 5. In Table 3, we assign to each of these crack paths the corresponding type. This classification will be also used in Section 4. Figure 6 depicts the corresponding energy-displacement curves. From the energy plots it may be concluded that the Type 1 (nearly vertical) crack path is not energetically favorable in comparison with Types 2 and 3 (curved paths). Also, the latter ones seem to have almost identical energy levels.

The computational time for the numerical experiment with $\Delta\bar{u} = 0.01$, depending on the mesh size, ranges from 6 to 14 hours on a standard desktop machine (Intel(R) Core(TM) i7-3770 OK, CPU 3.5 GHz, RAM 16.0 GB). Therefore, we test also the larger loading increment $\Delta\bar{u} = 0.1$. In Figure 7, the corresponding results are depicted. Our

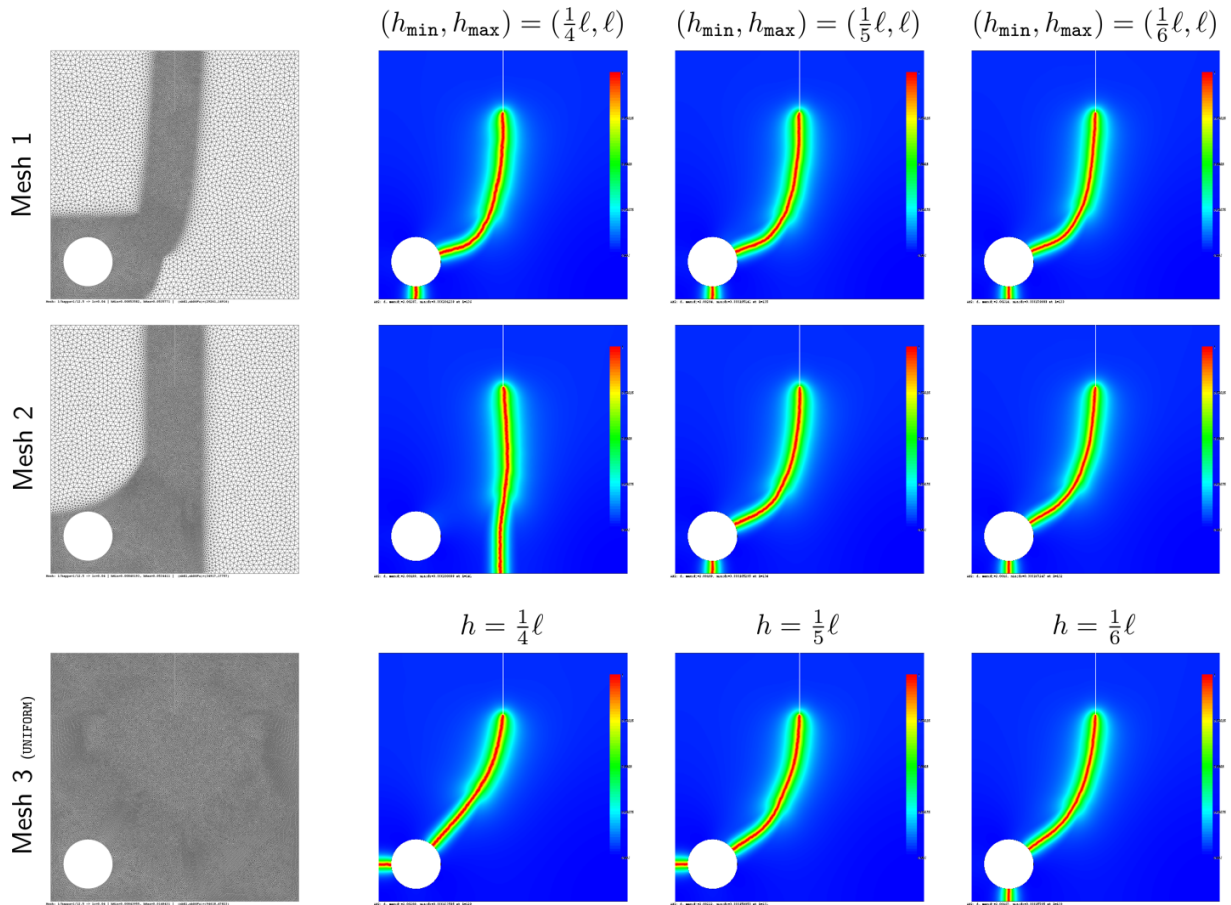


Figure 5: Computational results on three different mesh types with varying minimum mesh size for the loading increment $\Delta\bar{u} = 0.01$. Three different fracture mechanisms can be observed.

first observation is that the alteration of the loading increment while keeping the mesh type fixed can trigger solution non-uniqueness, as can be seen by comparing the results for, e.g. **Mesh 1** with $(h_{\min}, h_{\max}) = (\frac{1}{5}\ell, \ell)$ from Figures 5 and 7, respectively. Similar observations hold for **Mesh 2** with $(h_{\min}, h_{\max}) = (\frac{1}{5}\ell, \ell)$, and also for **Mesh 3** with $h = \frac{1}{4}\ell$ from the corresponding figures. Moreover, with the larger increment and regardless of the mesh type, we are capable to generate exactly the same three types of fracture mechanisms as in the previous case of $\Delta\bar{u} = 0.01$ but with a significantly lower computational effort: the time spent now ranges from 1 to 3 hours. Therefore, in the forthcoming stochastic modeling, which requires numerous realizations, the larger increment will be used.

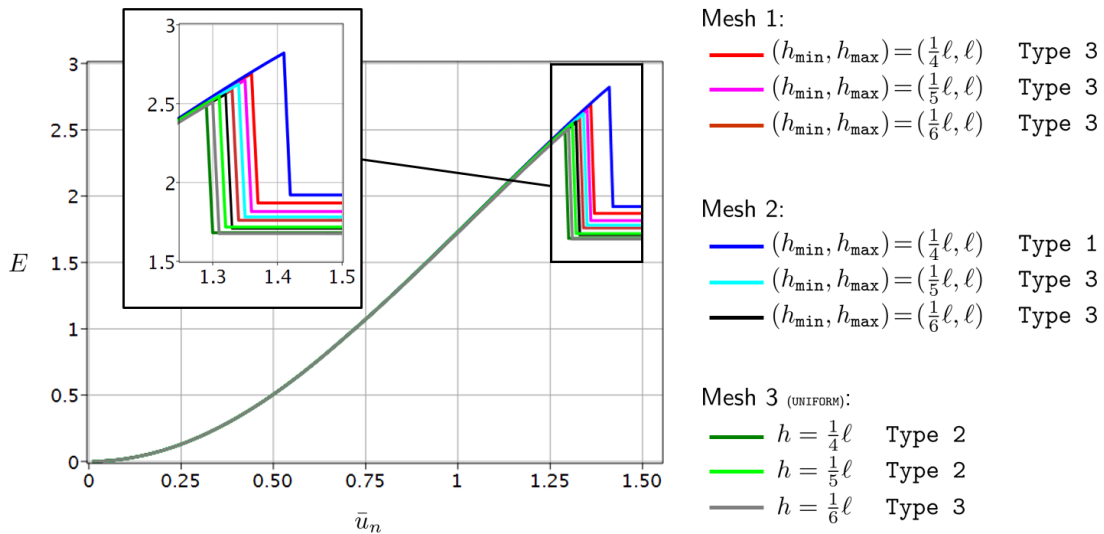


Figure 6: Energy-displacement plots for the solutions from Figure 5.

3 Stochastic modeling: some informal examples

This section is intended as an informal introduction to the ideas on how to model minimisation problems with multiple solutions in a relaxed setting, where we introduce perturbations of the functional and allow random variables as solutions. The first example deals with the minimisation of an ordinary function, whereas the next two examples address fracture of a 1D bar under tension, first with a sharp crack and then with a phase-field approach.

For these examples only rudimentary notions of probability are required, the details may be found in Subsection 4.1. All we need to know is that when x is a random variable (RV), and $\varphi(x)$ some function of this RV, the expectation of φ is $\mathbb{E}[\varphi] := \int \varphi(x) d\mathbb{P}$, where \mathbb{P} is the underlying probability measure.

3.1 Minimization of a double-well function

For a start, consider the example of the double-well function $E(x) = x^2(1-x)^2$ defined on the real line \mathbb{R} , which is not convex and has two global minima at the points $x = 0$ and $x = 1$ with value $E(0) = E(1) = 0$, and a local maximum at the point $x = 1/2$.

The original minimisation problem of finding $x = \arg \min_{y \in \mathbb{R}} E(y)$ with the solutions $x = 0$ and $x = 1$ will now be converted — relaxed — to a minimisation over RVs. We will perturb the function $E(\cdot)$ by a RV q to $E(q; \cdot)$ in such a way that $E(0; \cdot)$ is the original unperturbed function, and will be looking for minimisers of the expected value of E not in \mathbb{R} , but in some appropriate space \mathcal{X} of RVs with values in \mathbb{R} :

$$x = \arg \min_{y \in \mathcal{X}} E(y) = \arg \min_{y \in \mathcal{X}} \mathbb{E}[E(q; y)].$$

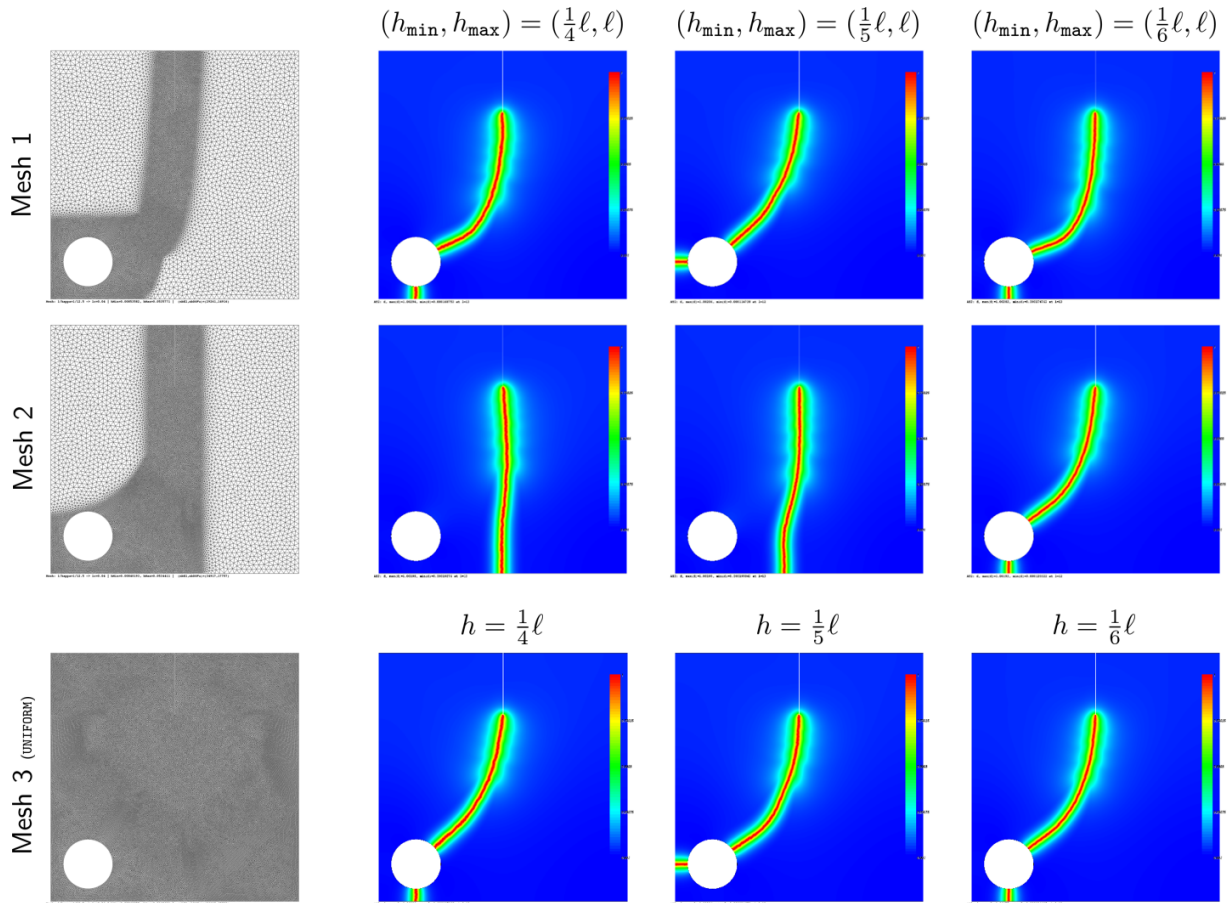


Figure 7: Computational results on three different mesh types with varying minimum mesh size for the loading increment $\Delta \bar{u} = 0.1$. Fracture mechanisms similar to those in Figure 5 are observed.

Here the new function is $E(y) = \mathbb{E}[E(q; y)]$, and we take as perturbation $E(q; x) = x^2 \cdot (1 - x)^2 + q \cdot x$. More generally, we are interested in

$$x(\eta) = \arg \min_{y \in \mathcal{X}} \mathbb{E}[E(\eta \cdot q; y)], \quad (12)$$

for $\eta > 0$ and in the limiting behaviour $\lim_{\eta \rightarrow +0} x(\eta)$.

We first consider the minimisation over \mathcal{X} without perturbation, i.e. $\eta = 0$. As the minimum of the function is still zero, it is not difficult to see that two solutions are the two — not really random — variables $x \equiv 0$ and $x \equiv 1$. In fact, any RV x which takes only the value 0 with probability $\mathbb{P}(x = 0) = p$ and the value 1 with probability $\mathbb{P}(x = 1) = 1 - p$ for any $p \in [0, 1]$ is a minimiser. As explained in Subsection 4.1, for a fixed $p \in [0, 1]$ all such RVs are considered as equivalent. Therefore, the probability distribution π_x of *any* minimiser x can be described as the convex combination of two Dirac point measures δ_x

located at the global minima $x = 0$ and $x = 1$, i.e.

$$\pi_x = p \delta_0 + (1 - p) \delta_1 \quad \text{for any } p \in [0, 1].$$

Let us consider now the perturbed (still non-convex) problem (12) with a bounded perturbing RV q and sufficiently small $0 \leq \eta \ll 1$. The perturbed function still has two local minima and in between a local maximum. Thus, for a positive realisation of the RV q the global minimum is still close to $x = 0$, and for a negative realisation of the RV q the global minimum is still close to $x = 1$, continuously dependent on η . Setting $\bar{p} := \mathbb{P}(q > 0)$, it is not difficult to see that the stochastic solution for $\eta \rightarrow +0$ is any RV x which takes only the values $x = 0$ with probability $\mathbb{P}(x = 0) = \bar{p}$ and $x = 1$ with probability $\mathbb{P}(x = 1) = 1 - \bar{p}$. Here it was tacitly assumed that the RV q takes the value 0 with vanishing probability: $\mathbb{P}(q = 0) = 0$. And as RVs which have the same distribution are considered equivalent, cf. Subsection 4.1, this now unique abstract RV has the limiting distribution

$$\pi_x = \bar{p} \delta_0 + (1 - \bar{p}) \delta_1,$$

where \bar{p} is a fixed number dependent on the RV q . Summing up, the limiting solution for the relaxed (stochastic) global minimization problem in this case is unique, and it depends on the perturbation q .

Thus far we considered the global minimization of $E(x)$. Let us now consider the relaxation of the corresponding deterministic stationarity condition $dE(x)/dx = 0$ with solutions at $x = 0, 1/2$, and 1. The Euler-Lagrange equation for the solution $x(\eta)$ is (cf. Subsection 4.2)

$$\mathbb{E}[\partial_x E(\eta \cdot q; x(\eta)) \cdot y] = 0 \quad \forall y \in \mathcal{X}. \quad (13)$$

With a bounded perturbing RV q and sufficiently small $0 \leq \eta \ll 1$, (13) has three solutions — stationary points of E — for any realisation of the RV q . Thus the solutions, which depend continuously on η , are still going to be close to $x = 0, 1/2$, and 1, which are the limiting solutions for $\eta \rightarrow +0$. Hence, any RV x which only takes the values $x = 0, 1/2$, and 1 with arbitrary probabilities $\mathbb{P}(x = 0) = p_0$, $\mathbb{P}(x = 1) = p_1$ (with $p_0 + p_1 \leq 1$), and $\mathbb{P}(x = 1/2) = (1 - p_0 - p_1)$ is a limiting solution, and the probability distribution π_x of any such limiting stationary solution x is

$$\pi_x = p_0 \delta_0 + (1 - p_0 - p_1) \delta_{1/2} + p_1 \delta_1.$$

The Euler-Lagrange equation can neither distinguish between maximum or minimum, nor between local and global minimum. Therefore the limiting solution for the relaxed (stochastic) stationarity problem embodied by the Euler-Lagrange equation in this case is not unique, and it does not depend on q .

3.2 Fracture of a 1D bar with a sharp crack approach

We next consider fracture of a 1D bar. This example is inspired by the study in [69] and similar localisation studies for gradient-based plasticity and damage models [70, 71, 72, 73].

Consider a bar of length L , with varying cross-section $A(x)$, fixed at one end and subjected to an increasing applied displacement at the other end. The energy functional of brittle fracture (1) is in this case with $D = [0, L]$:

$$E(u, \Gamma_c) = \frac{1}{2} \int_{D \setminus \Gamma_c} YA(x)(u'(x))^2 dx + \int_{\Gamma_c} G_c A(x) \mathbb{H}^0(dx),$$

where the Young's modulus Y and the critical energy release rate G_c are constant. $G_c A(x)$ is the fracture energy for a crack at x , and $\mathbb{H}^0(\Gamma_c)$ is the Hausdorff measure of the crack, a discrete measure equal to the number of crack points $\#\Gamma_c$. In the numerical tests we set $L = 6$. Note that although dimensionally $G_c A(x)$ is a dissipated energy, in this 1D example where fracture occurs at a point it can also be considered a dissipation density, and we will refer to it accordingly. In this example, due to the difficulty in dealing with the stationarity condition with respect to the unknown crack set Γ_c , we only consider the global minimization of the energy and its relaxed (stochastic) formulation.

The bar does not crack until the elastic energy $\frac{1}{2} \int_D YA(x)(u'(x))^2 dx$ reaches the minimum dissipation $\min_{x \in D} G_c A(x)$ with a single crack. A failure with multiple cracks cannot occur in the formulation with global minimisation of the energy because a higher dissipation would be required. Note that there is no need for a real computation, as the location of the crack $x_c = \arg \min_{x \in D} G_c A(x)$ depends only on the location of the minimum dissipation density.

Considering a variable dissipation density, see Figure 8(a), such as

$$G_c A(x) = \begin{cases} 1 + |x - 1| & \text{for } x < 2 \\ 1 + \frac{|x-4|}{2} & \text{for } x \geq 2 \end{cases}, \quad (14)$$

the bar breaks either at $x = 1$ or at $x = 4$. However, the probability of failure for individual points remains unknown. In order to obtain more information about these probabilities, we perturb the problem by random noise, which may reflect reality when e.g. the local behaviour is influenced by small heterogeneities.

Here the cross-sectional area $A(x)$ is perturbed with a white noise RV q with a uniform distribution supported on the interval $[-1/2, 1/2]$. Technically, at the discrete level at the grid points x_i the dissipation is set to $G_c A(x_i) + \eta \cdot q_i$, where the uniform RV q_i is independent of the RVs q_j at other grid points x_j , $j \neq i$, and $\eta > 0$ controls the magnitude of the perturbation. In particular, 1001 points were used in the discretisation of the computational interval $[0, 6]$.

The point of failure is simply computed as the minimum of the dissipation density. The histogram of failure points and the corresponding probability density (estimated through kernel density estimation) are shown in Fig 8(c,d). The failures occur in the neighbourhood of the points 1 and 4. However, the dissipation density has a different shape around those points, which results in different probability distributions. In particular, the probability of a failure around the point 1 is $1/3$, while it is $2/3$ around the point 4, independently of the perturbation parameter η . These results suggest the existence of a unique relaxed

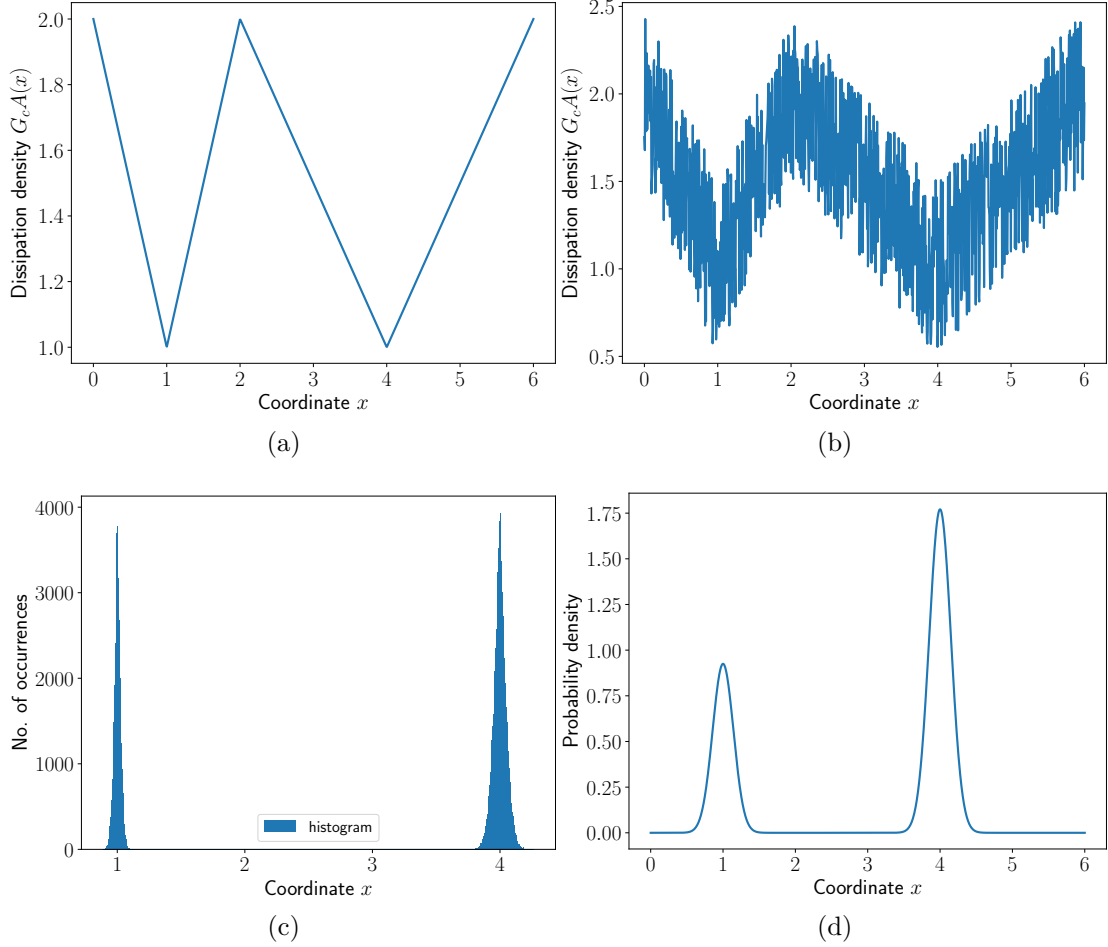


Figure 8: Distribution of (a) dissipation density and (b) discretised dissipation density perturbed by uniform white noise, (c) histogram of crack points with (d) corresponding estimation of the probability density function for $\eta = 0.01$. The probability of localisation is $1/3$ for the neighbourhood of $x = 1$, and $2/3$ for the neighbourhood of $x = 4$.

minimizer as the distribution

$$\pi_x = \frac{1}{3} \delta_1 + \frac{2}{3} \delta_4. \quad (15)$$

Note that the spatial discretisation has to be fine enough to obtain accurate numerical approximations of the probabilities for small perturbation parameters η .

In the first example the shape of the dissipation density curve was like two V-shaped notches. The next example has the dissipation density curve like two U-shaped notches, depicted in Figure 9, and defined as

$$G_cA(x) = \begin{cases} 1 + (x - 1)^2 & \text{for } x < 2 \\ 1 + \frac{1}{4}(x - 4)^2 & \text{for } x \geq 2 \end{cases}. \quad (16)$$

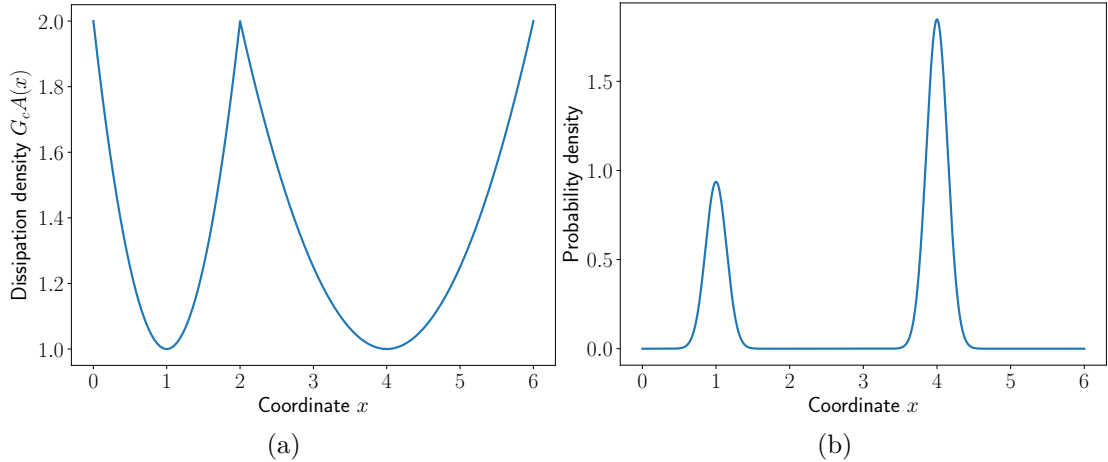


Figure 9: Distribution of (a) dissipation density and (b) probability density of the crack points for $\eta = 0.01$. The probability of localisation remains $1/3$ for the neighbourhood of $x = 1$, and $2/3$ for the neighbourhood of $x = 4$.

Similarly to the previous example, the different shape of the fracture dissipation density curve gives rise to a different distribution of the crack points. However, the probabilities that the crack is located either at $x = 1$ or $x = 4$ remain $1/3$ and $2/3$ respectively, and are again independent of the perturbation parameter η . Once again this suggests a unique relaxed minimizer as in (15).

The last example in this section has the dissipation density curve, shown in Fig. 10, in form of a U-shaped and V-shaped notch as

$$G_c A(x) = \begin{cases} 1 + (x - 1)^2 & \text{for } x < 2 \\ 1 + \frac{|x-4|}{2} & \text{for } x \geq 2 \end{cases}. \quad (17)$$

Contrary to the previous two examples, the localisation of the failure point is attracted to the point $x = 1$ for decreasing values of η , attaining the probability 1 in the limit, so that there seems to be a unique relaxed minimizer with distribution $\pi_x = \delta_1$.

3.3 Fracture of a 1D bar in the phase-field setting

The example of the previous Subsection 3.2 is now analyzed in the framework of phase field regularisation. The energetic functional then reads

$$E(u, \alpha) = \frac{1}{2} \int_0^L (1 - \alpha(x))^2 Y A(x) (u'(x))^2 dx + \frac{1}{2} \int_0^L G_c A(x) \left(\frac{\alpha^2(x)}{\ell} + \ell (\alpha'(x))^2 \right) dx.$$

Note that for this monotonic tension setup the irreversibility constraint for α does not need to be enforced as it is automatically satisfied. In the numerical tests we set $Y = 10^4$, $L = 6$ and use $G_c A(x)$ as given in (14), i.e. the double V-notch case. A uniform finite element

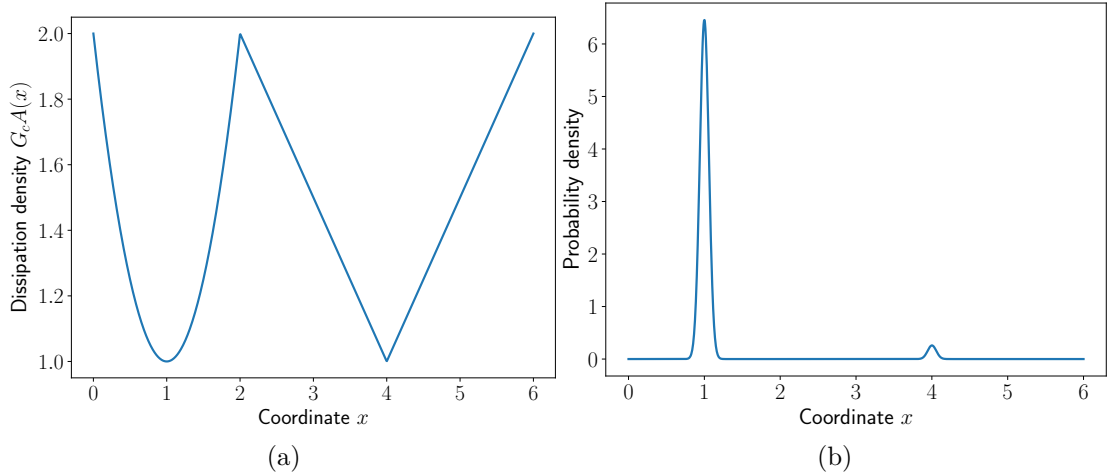


Figure 10: Distribution of (a) dissipation density, and (b) probability density of the crack points for $\eta = 0.01$. The probability of localisation is attracted to the neighbourhood of $x = 1$ with limiting probability equal to 1.

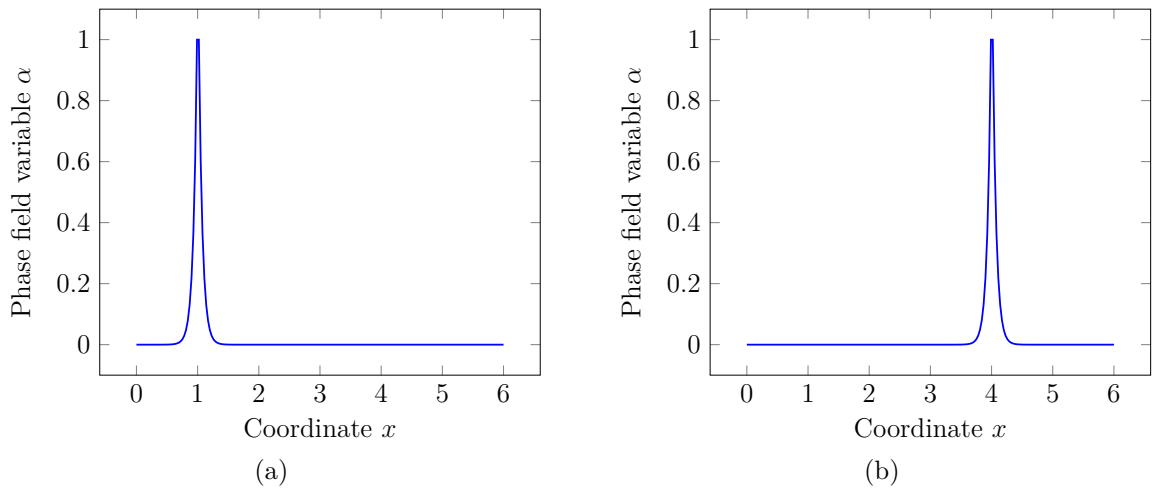


Figure 11: Different crack types for the 1D phase field example.

mesh in $[0, L]$ is employed. The loading step is chosen as $\Delta u = 0.1$ and we consider 10 loading steps in total. At every fixed step, the staggered iterative solution process is carried out until $|\boldsymbol{\alpha}^{(k+1)} - \boldsymbol{\alpha}^{(k)}| < 10^{-4}$, where $\boldsymbol{\alpha}^{(k)}$ represents the nodal phase field values $|\cdot|$ is the Euclidean norm.

Unlike in the previous example, here we look for solutions which correspond to local minima (or even stationary points) of the energy, as our numerical procedure solves the Euler-Lagrange equations. For a thorough discussion of the differences between predictions of the two approaches in the context of fracture, see [24]. The perturbation of $G_c A(x)$ is generated in the same way as in Section 3.2: at the grid nodes x_i the dissipation is set to

$G_c A(x_i) + \eta \cdot q_i$ with q_i denoting pairwise independent and uniformly distributed random numbers in the interval $[-1/2, 1/2]$. Then, a piecewise linear interpolation is used to obtain the perturbed $G_c A(x)$. Since computations are more expensive here than in the previous two examples, we choose a smaller sample size, but monitor the sampling accuracy with the 95% confidence interval $\Delta_{0.95} = 1.96 \sqrt{p_i(1-p_i)}/M$, $i = 1, 2$, see [81]. Note that p_1 and p_2 represent the probabilities of cracks occurring at $x = 1$ and $x = 4$, respectively. Figure 11 depicts the two cracks appearing in this scenario.

η	ℓ	# grid points	p_1	p_2
1	$0.1L$	500	0	1
1	$0.01L$	1000	0.24	0.76
1	$0.001L$	2000	0.33	0.67
0.5	$0.01L$	1000	0.11	0.89
0.5	$0.001L$	2000	0.32	0.68
0.5	$0.0001L$	5000	0.34	0.66
0.1	$0.01L$	1000	0	1
0.1	$0.001L$	2000	0.24	0.76
0.1	$0.0001L$	5000	0.34	0.66

Table 4: Crack probabilities obtained with the phase field approach and Monte Carlo sampling for varying perturbation size, regularization length and grid interval size. In all cases, the sample size is $M = 2500$ and for the sampling error there holds $\Delta_{0.95} \leq 0.02$.

Table 4 shows the computed probabilities for different perturbation magnitudes. For all settings a sample size of $M = 2500$ has been employed for which the 95% confidence interval is smaller than 0.02. The results reveal that the regularization length ℓ and the mesh interval size have to be chosen small enough to capture the stochastic perturbations. For instance, when a relatively large perturbation ($\eta = 1$) is resolved with $\ell = 0.01L$ and 1000 grid points (the same number of points as in Section 3.2), we observe a bias in the computed probabilities. Only after refining ℓ and the mesh size we obtain $p_1 = 1/3$ and $p_2 = 2/3$, as expected. Note that when ℓ is decreased, a finer mesh is needed to properly resolve the regularized cracks. The same observations can be made for smaller perturbation amplitudes, where the mesh interval size and ℓ have to be successively refined to recover $p_1 = 1/3$ and $p_2 = 2/3$. If the resolution is much too coarse, only cracks at $x = 4$ are observed, since the perturbation cannot be resolved by the phase field finite element method. Indeed, a crack at $x = 4$ is also obtained for our specific implementation in this example, if all coefficients are deterministic. These results suggest that there exists again a unique relaxed minimizer as in (15).

4 Stochastic phase-field modeling of brittle fracture

As mentioned earlier, the minimisation of non-convex energy functionals such as (2) may produce local minima. Especially when the energy levels of these competing minima are close, little random perturbations in the physical system and/or in the numerical setup may lead to different solutions as has been demonstrated in the examples shown. This is further complicated by the fact that the necessary condition (6) of the vanishing first variation has all stationary points of the functional as solutions. The idea is therefore to relax the minimisation problem in such a way as to hopefully capture all these possibilities. This will be done explicitly by assuming some random perturbations in the energy functional (2) by allowing some quantity specifying the functional to be a RV, or more generally a random field (RF).

In this way, the energy functional (2) becomes a RV, and one has to specify what it means to minimise it. Here, guided by previous work on variational stochastic extensions for elasticity [55, 56, 57] as well as for plasticity [58, 59, 60] in a convex analysis framework, a new stochastic energy functional is defined as the expected value of the randomised deterministic energy functional (2). From here on things can proceed in a theoretically analogous manner to the deterministic formulation in section 2.1.

In this section, we first introduce some necessary concepts on RVs and probability. Then, we formulate the proposed stochastic phase-field model and computational framework for brittle fracture, which we finally illustrate with numerical results.

4.1 Preliminaries

As follows, we briefly introduce the concepts and the notation needed for the formulation of the proposed stochastic phase-field model in the following section.

4.1.1 Random variables and random fields

We start with the familiar concept of scalar or real valued random variables (RVs) and their expectation. Formally (see e.g. [61]), such RVs can be represented as measurable real valued functions on a probability space $(\Theta, \mathfrak{G}, \mathbb{P})$, where Θ is the set of all possible samples or realisations, and \mathfrak{G} is a σ -algebra of measurable subsets of Θ — the so-called events — on which the probability measure \mathbb{P} is defined.

What is important here for our purposes is that such random variables (RVs) form a vector space on which the expectation is defined as a positive linear functional via the integral w.r.t. the probability measure, which for such a RV $a : \Theta \rightarrow \mathbb{R}$ is given in the usual way by $\mathbb{E}[a] := \int_{\Theta} a(\theta) \mathbb{P}(d\theta) \in \mathbb{R}$. In case the RV a has a density f_a on its range \mathbb{R} , one also has the familiar relation $\mathbb{E}[a] = \int_{\mathbb{R}} \eta f_a(\eta) d\eta$. Note that the probability of some event $\mathcal{E} \in \mathfrak{G}$ can be stated as an expectation $\mathbb{P}(\mathcal{E}) = \mathbb{E}[\mathbb{1}_{\mathcal{E}}]$, where the indicator or characteristic function of \mathcal{E} is a RV which takes the value one ($\mathbb{1}_{\mathcal{E}}(\theta) = 1$) if $\theta \in \mathcal{E}$, and vanishes otherwise. The mean of a RV a is often denoted by $\bar{a} := \mathbb{E}[a] \in \mathbb{R}$, and the mean-free fluctuating

random part by $\tilde{a} := a - \bar{a}$. The real RVs form not only a vector space, but an algebra, as one may define a product simply in the usual way by point-wise multiplication, and in this way obtain an inner product $\langle a | b \rangle_{\mathcal{S}} := \mathbb{E}[ab]$. The usual Hilbert Lebesgue space of RVs with finite variance, which will be used later, is denoted by

$$\mathcal{S} := L_2(\Theta; \mathbb{R}) = \{a : \Theta \rightarrow \mathbb{R} : \|a\|_{\mathcal{S}}^2 := \langle a | a \rangle_{\mathcal{S}} = \mathbb{E}[a^2] < \infty\}. \quad (18)$$

For RVs $a, b \in \mathcal{S}$ the covariance is given by $\text{cov}(a, b) := \langle \tilde{a} | \tilde{b} \rangle_{\mathcal{S}} = \mathbb{E}[\tilde{a}\tilde{b}]$, and the variance and standard deviation by $\text{var}(a) := \text{cov}(a, a) = \|\tilde{a}\|_{\mathcal{S}}^2 = \langle \tilde{a} | \tilde{a} \rangle_{\mathcal{S}} = \mathbb{E}[\tilde{a}^2]$ and $\text{std}(a) := \sqrt{\text{var}(a)}$. In case $\text{cov}(a, b) = 0$, the RVs a and b are called *uncorrelated*.

Two RVs a_1 and a_2 , possibly defined on different probability spaces Θ_1 and Θ_2 , are considered equivalent if $\mathbb{E}[\varphi(a_1)] = \mathbb{E}[\varphi(a_2)]$ for all functions φ where that expression makes sense. This means in particular that equivalent RVs have the same distribution and moments. Similarly, two such RVs are independent if

$$\mathbb{E}[\varphi(a_1)\varphi(a_2)] = \mathbb{E}[\varphi(a_1)]\mathbb{E}[\varphi(a_2)]$$

for all functions φ where that expression makes sense. Note that independent RVs are always uncorrelated, but the reverse implication may not hold.

The next task is to formalise RFs, e.g. RVs with values in the Hilbert Sobolev space \mathcal{P} in (5). These will be possible candidates for minimisers of the stochastic variational formulation, and such RFs are also used to perturb the energy functional and are an input to the stochastic formulation and computation. A RF $\mathbf{a}(\theta, \mathbf{x}) : \Theta \times D \rightarrow \mathbb{R}$ is a function of two arguments, namely $\theta \in \Theta$ as the stochastic variable and $\mathbf{x} \in D$ as the spatial variable. For $\hat{\theta} \in \Theta$ fixed, $\mathbf{a}(\hat{\theta}) := \mathbf{a}(\hat{\theta}, \cdot)$ is a deterministic phase field which we will want to be in \mathcal{P} , whereas on the other hand, for $\hat{\mathbf{x}} \in D$ fixed, $\mathbf{a}(\cdot, \hat{\mathbf{x}})$ is a real valued RV which we will want to be in $\mathcal{S} = L_2(\Theta; \mathbb{R})$.

4.1.2 Random phase fields

As very general RVs with values in an infinite dimensional Hilbert space may pose some unexpected mathematical difficulties, we restrict ourselves to a somewhat simple situation [62, 57] which is general enough to display the idea. From the Hilbert space \mathcal{S} of RVs in (18) and the Hilbert space $\mathcal{P} = H^1(D; \mathbb{R})$ in (5) of deterministic phase fields with the usual Sobolev inner product $\langle \cdot | \cdot \rangle_{\mathcal{P}}$, we form a new Hilbert space of random phase fields (RFs) as the Hilbert tensor product of possible solutions to the stochastic variational problem (cf. [62, 57, 60])

$$\mathcal{P} := \mathcal{S} \otimes \mathcal{P} \quad \text{with usual inner product} \quad \langle \mathbf{a} | \mathbf{b} \rangle_{\mathcal{P}} := \langle a | b \rangle_{\mathcal{S}} \langle \alpha | \beta \rangle_{\mathcal{P}} \quad (19)$$

for elementary tensors $\mathbf{a} = a \otimes \alpha, \mathbf{b} = b \otimes \beta \in \mathcal{P} := \mathcal{S} \otimes \mathcal{P}$, where for example in $\mathbf{a} = a \otimes \alpha$ — $(\mathbf{a}(\theta, \mathbf{x}) = a(\theta)\alpha(\mathbf{x}))$ — the factor $a \in \mathcal{S}$ is a RV and the factor $\alpha \in \mathcal{P}$ is a deterministic phase field. As the whole space \mathcal{P} is composed of sums and convergent series

$\sum_j a_j \otimes \alpha_j$ of such elementary tensors, the inner product in (19) is extended by linearity to the whole space. Note that (19) implies that the induced \mathcal{P} -norm is a cross norm: $\|\mathbf{a}\|_{\mathcal{P}} = \|a\|_{\mathcal{S}} \|\alpha\|_{\mathcal{P}}$. If the \mathcal{P} -inner product and -norm are extended to \mathcal{P} in the obvious fashion, namely for elementary tensors like above $\langle \mathbf{a}(\theta, \cdot) | \mathbf{b}(\theta, \cdot) \rangle_{\mathcal{P}} := a(\theta)b(\theta) \langle \alpha | \beta \rangle_{\mathcal{P}}$ and $\|\mathbf{a}(\theta, \cdot)\|_{\mathcal{P}} = |a(\theta)| \|\alpha\|_{\mathcal{P}}$, then $\langle\langle \mathbf{a} | \mathbf{b} \rangle\rangle_{\mathcal{P}} = \mathbb{E}[\langle \mathbf{a} | \mathbf{b} \rangle_{\mathcal{P}}]$ and $\|\mathbf{a}\|_{\mathcal{P}} = \mathbb{E}[\|\mathbf{a}\|_{\mathcal{P}}]$, i.e. the quantities on the stochastic space \mathcal{P} are just the expectations of the ones on the base space \mathcal{P} , a pattern which will be repeated several times.

Similarly, the expectation as a linear map to the basis space \mathcal{P} of deterministic fields is defined on \mathcal{P} by $\bar{\mathbf{a}} = \mathbb{E}[\mathbf{a}] := \mathbb{E}[a]\alpha \in \mathcal{P}$ on elementary tensors $\mathbf{a} = a \otimes \alpha \in \mathcal{P}$, and extended to all of \mathcal{P} by linearity. It is well known [61] that the tensor product space \mathcal{P} in (19) is isomorphic with the Hilbert space of RFs $\mathbf{a} : \Theta \rightarrow \mathcal{P}$ where the \mathcal{P} -norm has finite variance

$$\begin{aligned} \mathcal{P} &= \mathcal{S} \otimes \mathcal{P} = L_2(\Theta; \mathbb{R}) \otimes H^1(D; \mathbb{R}) \cong L_2(\Theta; \mathcal{P}) = L_2(\Theta; H^1(D; \mathbb{R})) \\ &= \{\mathbf{a} : \|\mathbf{a}\|_{\mathcal{P}}^2 := \langle\langle \mathbf{a} | \mathbf{a} \rangle\rangle_{\mathcal{P}} = \mathbb{E}[\langle \mathbf{a} | \mathbf{a} \rangle_{\mathcal{P}}] = \mathbb{E}[\|\mathbf{a}\|_{\mathcal{P}}^2] < \infty\}. \end{aligned} \quad (20)$$

4.1.3 Quantities of interest

A quantity of interest (QoI) in the deterministic setting is typically some function $\Upsilon(\mathbf{u}, \alpha)$ of the solution $(\mathbf{u}, \alpha) \in \mathcal{U}_n \times \mathcal{P}_n$. Now if in the stochastic formulation the deterministic fields (\mathbf{u}, α) are replaced by RFs (\mathbf{u}, \mathbf{a}) , and inserted into the deterministic QoI $\Upsilon(\mathbf{u}, \mathbf{a})$, this becomes a RV. One is then typically interested in a new QoI like $\Upsilon(\mathbf{u}, \mathbf{a}) := \mathbb{E}[\Upsilon(\mathbf{u}, \mathbf{a})]$, where Υ is an appropriate function. Some examples are the mean $\bar{\mathbf{a}} = \mathbb{E}[\mathbf{a}]$ with $\Upsilon(\mathbf{u}, \mathbf{a}) = \mathbf{a}$, or the p -th central moment $\mathbb{E}[(\mathbf{a} - \mathbb{E}[\mathbf{a}])^p]$ with $\Upsilon(\mathbf{u}, \mathbf{a}) = (\mathbf{a} - \bar{\mathbf{a}})^p$. As already mentioned, in general a pattern is that the probabilistic QoI is the expected value of the deterministic QoI.

4.1.4 Separated representation

The relations (19) and (20) give also a practical way of approximating RFs in a *separated representation* as linear combinations $\mathbf{a}(\theta, \mathbf{x}) \approx \sum_j a_j(\theta) \alpha_j(\mathbf{x})$ of deterministic fields $\alpha_j \in \mathcal{P}$ with RVs $a_j \in \mathcal{S}$ as coefficients. Such separated expansions are typical for parametric maps $\mathbf{a} : \Theta \rightarrow \mathcal{P}$ from a set Θ into a Hilbert space \mathcal{P} , which can be analysed very generally in terms of linear operators [63]. This kind of analysis was started in probability theory in [64, 52, 53] in terms of the so-called Karhunen-Loève expansion [61]. It begins by defining for a RF \mathbf{a} a bilinear form for any $(\beta_1, \beta_2) \in \mathcal{P} \times \mathcal{P}$ by

$$\mathbb{E}[\langle \tilde{\mathbf{a}}, \beta_1 \rangle \langle \tilde{\mathbf{a}}, \beta_2 \rangle] = \langle C_{\mathbf{a}} \beta_1, \beta_2 \rangle = \iint_{D \times D} \beta_1(\mathbf{x}) \text{cov}_{\mathbf{a}}(\mathbf{x}, \mathbf{y}) \beta_2(\mathbf{y}) \, d\mathbf{x} \, d\mathbf{y},$$

which in turn defines the self-adjoint positive semi-definite *covariance operator* $C_{\mathbf{a}} : \mathcal{P} \rightarrow \mathcal{P}^*$ and the symmetric positive semi-definite correlation function $\text{cov}_{\mathbf{a}} : D \times D \rightarrow \mathbb{R}$. This shows that $C_{\mathbf{a}}$ can be represented as an integral operator, and its eigenvalues equal those

of the integral operator with kernel equal to cov_a . As $\text{cov}_a(\mathbf{x}, \mathbf{y}) = \mathbb{E}[\tilde{\mathbf{a}}(\cdot, \mathbf{x})\tilde{\mathbf{a}}(\cdot, \mathbf{y})] = \langle \tilde{\mathbf{a}}(\cdot, \mathbf{x}) | \tilde{\mathbf{a}}(\cdot, \mathbf{y}) \rangle_{\mathcal{S}} = \text{cov}(\mathbf{a}(\cdot, \mathbf{x}), \mathbf{a}(\cdot, \mathbf{y}))$, it is easily seen that the local variance and standard variation at $\mathbf{x} \in D$ are $\text{var}_a(\mathbf{x}) = \text{cov}_a(\mathbf{x}, \mathbf{x})$ and $\text{std}_a(\mathbf{x}) = \sqrt{\text{var}_a(\mathbf{x})}$, and the total variance of the RF \mathbf{a} is defined as

$$\mathbb{V}(\mathbf{a}) := \mathbb{E}[\langle \tilde{\mathbf{a}}, \tilde{\mathbf{a}} \rangle] = \int_D \text{var}_a(\mathbf{x}) \, d\mathbf{x} = \int_D \text{cov}_a(\mathbf{x}, \mathbf{x}) \, d\mathbf{x} = \text{tr } C_a < \infty. \quad (21)$$

This means that C_a is a compact operator, where the sum of eigenvalues (the trace) is finite, i.e. C_a is a trace-class or nuclear operator, and thus the RF $\mathbf{a} \in \mathcal{P}$ represents a proper RV, i.e. a measurable map $\mathbf{a} : \Theta \rightarrow \mathcal{P}$ [61]. The eigenvalue equation for $C_a(\varphi_j)(\mathbf{x}) = \int_D \text{cov}_a(\mathbf{x}, \mathbf{y}) \varphi_j(\mathbf{y}) \, d\mathbf{y} = \lambda_j \varphi_j(\mathbf{x})$ then leads to the celebrated Karhunen-Loève expansion [64, 52, 53, 61], a separated expansion in terms of orthogonal eigenfunctions of C_a :

$$\mathbf{a}(\theta, \mathbf{x}) = \bar{\mathbf{a}}(\mathbf{x}) + \sum_{j=1}^{\infty} \sqrt{\lambda_j} \zeta_j(\theta) \varphi_j(\mathbf{x}). \quad (22)$$

This expansion can be shown to correspond to a singular value decomposition [63]. The uncorrelated zero mean unit variance RVs $\zeta_j \in \mathcal{S}$ are given by orthogonal projection $\zeta_j(\theta) = \langle \tilde{\mathbf{a}}(\theta, \cdot), \varphi_j \rangle = \int_D \tilde{\mathbf{a}}(\theta, \mathbf{y}) \varphi_j(\mathbf{y}) \, d\mathbf{y}$. Arranging the eigenvalues λ_j of C_a in a descending order, the truncation of the Karhunen-Loève series (22) after J terms gives the *best* J -term approximation to \mathbf{a} , and is often used in the generation resp. sampling of RFs.

4.1.5 Random displacement fields

A completely analogous construction is carried out for the displacements, so that one arrives at a Hilbert space of stochastic displacement variations $\mathcal{U} = \mathcal{S} \otimes \mathcal{U}$ as the probabilistic analogue of the deterministic Hilbert space \mathcal{U} in (7). In particular, as the deterministic space \mathcal{U} is a space of \mathbb{R}^d -valued fields the space \mathcal{U} will be a Hilbert space with \mathbb{R}^d -valued RFs. The inner product on the deterministic space \mathcal{U} can be taken as $\langle \mathbf{u} | \mathbf{v} \rangle_{\mathcal{U}} = \int_D \text{tr}(\nabla \mathbf{u}(\mathbf{x})^T \cdot \nabla \mathbf{v}(\mathbf{x})) \, d\mathbf{x}$, and on the stochastic space \mathcal{U} it is in analogy to (19) defined for elementary tensors $\mathbf{u} = u \otimes \mathbf{u}, \mathbf{v} = v \otimes \mathbf{v} \in \mathcal{U} = \mathcal{S} \otimes \mathcal{U}$ as $\langle \langle \mathbf{u} | \mathbf{v} \rangle \rangle_{\mathcal{U}} := \langle u | v \rangle_{\mathcal{S}} \langle \mathbf{u} | \mathbf{v} \rangle_{\mathcal{U}} = \mathbb{E}[\langle \mathbf{u} | \mathbf{v} \rangle_{\mathcal{U}}]$, and extended by linearity. Once again one has a congruence like (20):

$$\begin{aligned} \mathcal{U} &= \mathcal{S} \otimes \mathcal{U} = L_2(\Theta; \mathbb{R}) \otimes H_T^1(D; \mathbb{R}^d) \\ &\cong L_2(\Theta; \mathbb{R}) \otimes H_T^1(D; \mathbb{R}) \otimes \mathcal{F} \cong L_2(\Theta; \mathcal{U}) = L_2(\Theta; H_T^1(D; \mathcal{F})) \\ &= \{ \mathbf{v} : \|\mathbf{v}\|_{\mathcal{U}}^2 := \langle \langle \mathbf{v} | \mathbf{v} \rangle \rangle_{\mathcal{U}} = \mathbb{E}[\langle \mathbf{v} | \mathbf{v} \rangle_{\mathcal{U}}] = \mathbb{E}[\|\mathbf{v}\|_{\mathcal{U}}^2] < \infty \}. \end{aligned} \quad (23)$$

All the other following constructions can be carried out in a completely analogous fashion to the ones for the space of random phase fields \mathcal{P} and need not be repeated here.

4.1.6 Stochastic constraints

It remains to define the stochastic analogues of the affine space \mathcal{U}_n in (4) and the convex set \mathcal{P}_n in (5). These will be used in the stochastic variational problems to be considered in Section 4.2. The stochastic affine space \mathcal{U}_n is defined as

$$\mathcal{U}_n := \{\mathbf{u} \in L_2(\Theta; H^1(D; \mathbb{R}^d)) : [\mathbf{u}(\theta, \mathbf{x}) = 0 \text{ on } \Gamma_{\text{Dir},0} \text{ and } \mathbf{u}(\theta, \mathbf{x}) = \bar{\mathbf{u}}_n \text{ on } \Gamma_{\text{Dir},1}] \mathbb{P} - \text{a.s.}\} \quad (24)$$

The stochastic analogue of the convex subset $\mathcal{P}_n \subset \mathcal{P}$ is again a convex subset of \mathcal{P} , and is defined as

$$\mathcal{P}_n := \{\mathbf{a} \in \mathcal{P} : [\mathbf{a}(\theta, \cdot) \geq \mathbf{a}_{n-1}(\theta, \cdot)] \mathbb{P} - \text{a.s.}\} \subset \mathcal{P}, \quad (25)$$

where $\mathbf{a}_{n-1} \in \mathcal{P}$ is known from the previous time step. In stochastic optimisation, when a previously deterministic constraint condition becomes random, it is often a question which would be the best way to enforce this condition in the stochastic case [80]. Observe that it could also be regarded as reasonable that instead of requiring e.g. in (24) that $\mathbf{u}(\theta, \mathbf{x}) = 0$ on $\Gamma_{\text{Dir},0}$ almost surely (a.s.) in the measure \mathbb{P} — i.e. that the probability of this condition being violated vanishes — one demands that only $\mathbb{E}[\mathbf{u}(\cdot, \mathbf{x})] = 0$ on $\Gamma_{\text{Dir},0}$. This would have been a much laxer condition, but the formulation in (24) seems to be a natural generalisation of (4), and demands the strict enforcement of the boundary condition for every realisation.

4.2 Stochastic formulation of the variational problem

The stochastic variational formulation to be presented here first needs to introduce some probabilistic notion into the minimisation problem (3). This will be achieved by a small random perturbation in the definition of the functional $E(\mathbf{u}, \alpha)$ by letting some variable or field \mathbf{q} which appears in the definition of E become a RV or RF \mathbf{q} . This way the functional now has become a RV. The second ingredient then will be to allow the solutions (\mathbf{u}, α) to be RFs (\mathbf{u}, \mathbf{a}) and define a new functional as the expectation of the deterministic one.

This is then the setting for the stochastic variational problem. It is a new real valued functional which has to be minimised over random fields. The necessary conditions for this will be derived similarly to (6) for the deterministic minimisation problem (3). Thus, in this general case such as in the 1D example of Section 3.3, we pursue the local minimization (or even the stationarity) problem and not the global minimization problem.

Let us start by choosing some quantity \mathbf{q} which appears in the definition of $E(\mathbf{u}, \alpha) = E(\mathbf{q}; \mathbf{u}, \alpha)$ to be perturbed. This choice obviously depends on the particular form of the energy functional E . Then this quantity is replaced by a random one \mathbf{q} , and the new functional is now a RV $E(\mathbf{q}; \mathbf{u}, \alpha)$, since \mathbf{q} is random. Following [55, 56, 57, 58, 59, 60] we choose the new energy functional to be the expected value of the deterministic one. The last ingredient is to allow RFs (\mathbf{u}, \mathbf{a}) to be the solution. With the preparations in the previous Section 4.1 and in particular with the definition of the admissible sets of RFs \mathcal{U}_n

in (24) and \mathcal{P}_n in (25), the new minimisation problem reads as follows:

$$(\mathbf{u}, \mathbf{a}) = \arg \min \{E(\mathbf{v}, \mathbf{b}) : \mathbf{v} \in \mathcal{U}_n, \mathbf{b} \in \mathcal{P}_n\}, \quad (26)$$

$$\text{with } E(\mathbf{v}, \mathbf{b}) = \mathbb{E}[E(\mathbf{q}; \mathbf{v}, \mathbf{b})]. \quad (27)$$

As formally the situation is completely equal to the deterministic case, the derivation of the necessary conditions is the same, giving in analogy to (6)

$$\begin{cases} \langle\langle \delta_{\mathbf{u}} E(\mathbf{u}, \mathbf{a}), \mathbf{v} \rangle\rangle := \mathbb{E}[\langle \delta_{\mathbf{u}} E(\mathbf{q}; \mathbf{u}, \mathbf{a}), \mathbf{v} \rangle] = 0 & \forall \mathbf{v} \in \mathcal{U}, \\ \langle\langle \delta_{\mathbf{a}} E(\mathbf{u}, \mathbf{a}), \mathbf{b} - \mathbf{a} \rangle\rangle = \mathbb{E}[\langle \delta_{\mathbf{a}} E(\mathbf{q}; \mathbf{u}, \mathbf{a}), \mathbf{b} - \mathbf{a} \rangle] \geq 0 & \forall \mathbf{b} \in \mathcal{P}_n, \end{cases} \quad (28)$$

where we recall that $\delta_{\mathbf{u}} E$ and $\langle \cdot, \cdot \rangle$ refer to the partial Gâteaux derivative of E and the dual pairing between the deterministic spaces \mathcal{U}^* and \mathcal{U} , respectively, whereas $\delta_{\mathbf{u}} E$ is the partial Gâteaux derivative of the new functional E , and $\langle\langle \cdot, \cdot \rangle\rangle := \mathbb{E}[\langle \cdot, \cdot \rangle]$ is the duality pairing between the stochastic spaces \mathcal{U}^* and \mathcal{U} . As an example pointing towards computation, from the first relation in (28) one can obtain a “strong version” w.r.t \mathcal{U} , which applies \mathbb{P} -almost surely (\mathbb{P} -a.s.):

$$\langle \delta_{\mathbf{u}} E(\mathbf{q}(\theta); \mathbf{u}(\theta), \mathbf{a}(\theta)), \mathbf{v}(\theta) \rangle = 0 \quad \forall \mathbf{v} \in \mathcal{U} \quad \mathbb{P} - \text{a.s.} \quad (29)$$

As \mathbb{P} -a.s. one has $\mathbf{u}(\theta) \in \mathcal{U}_n$ and $\mathbf{v}(\theta) \in \mathcal{U}$ — this means that except for θ in a set of vanishing probability — both the constraint (4) and the first of the governing equations in (6) is satisfied like in the deterministic case. A similar statement can be made about the second relation in (28) satisfying \mathbb{P} -a.s. the second relation in (6). These \mathbb{P} -a.s. statements are possible due to the \mathbb{P} -a.s. enforcement of the conditions in the definition of \mathcal{U}_n in (24) and \mathcal{P}_n in (25).

To be more specific, this general development is now applied to the definition of the functional from (2), for the sake of simplicity without the Neumann boundary term. The perturbed functional is

$$\begin{aligned} E(\mathbf{q}(\theta); \mathbf{u}(\theta), \mathbf{a}(\theta)) &= \int_D g(\mathbf{a}(\theta, \mathbf{x})) \Psi(\mathbf{q}(\theta); \boldsymbol{\varepsilon}(\mathbf{u}(\theta, \mathbf{x}))) \, d\mathbf{x} \\ &\quad + \frac{G_c}{c_w} \int_D \left(\frac{w(\mathbf{a}(\theta, \mathbf{x}))}{\ell} + \ell |\nabla \mathbf{a}(\theta, \mathbf{x})|^2 \right) \, d\mathbf{x} \end{aligned} \quad (30)$$

where we have assumed to perturb the elastic strain energy density Ψ . Then with (30) one has from (28):

$$\langle\langle \delta_{\mathbf{u}} E(\mathbf{u}, \mathbf{a}), \mathbf{v} \rangle\rangle = \mathbb{E} \left[\int_D g(\mathbf{a}(\cdot, \mathbf{x})) \partial_{\boldsymbol{\varepsilon}} \Psi(\mathbf{q}(\cdot); \boldsymbol{\varepsilon}(\mathbf{u}(\cdot, \mathbf{x}))) : \boldsymbol{\varepsilon}(\mathbf{v}(\cdot, \mathbf{x})) \, d\mathbf{x} \right] = 0 \quad \forall \mathbf{v} \in \mathcal{U}.$$

In particular, for the example of anti-plane shear, this Gâteaux derivative, corresponding to (10) in the deterministic case, becomes

$$\langle\langle \delta_{\mathbf{u}} E(\mathbf{u}, \mathbf{a}), \mathbf{v} \rangle\rangle = \mathbb{E} \left[\int_D (1 - \mathbf{a}(\cdot, \mathbf{x}))^2 \mu(\mathbf{q}(\cdot)) \nabla \mathbf{u}(\cdot, \mathbf{x}) \cdot \nabla \mathbf{v}(\cdot, \mathbf{x}) \, d\mathbf{x} \right],$$

where we have assumed a perturbation in the shear modulus μ . Obviously, the “strong version” resulting from (29) could also be written out for these particular cases; \mathbb{P} -a.s. for $\theta \in \Theta$ it just looks like the corresponding deterministic case.

4.3 Some remarks about Young measures

Here we briefly offer some remarks about Young measures (YM), which are used as a mathematical tool to generalise and relax variational formulations [43, 44], as well as “statistical solutions” [75], lately described by multi-point generalisations of YM [42, 38], and their relation to the here proposed concept of “stochastic solutions”.

Originally, the concept of YM was introduced to describe oscillation effects and was extended to include concentration effects (DiPerna-Majda measures [50]) of minimising sequences in variational formulations which lack minimisers. As an example, one can consider

$$\min_{u \in H_0^1((0,1))} \int_0^1 u^2 + [(u')^2 - 1]^2$$

which generates approximate minimisers close to zero with finer and finer slopes, i.e. an oscillating derivative $u' = \pm 1$; however, such functions are not contained in the space H_0^1 . This can be relaxed with YMs, which are parametrised probability measures $\mathbf{x} \mapsto \nu_{\mathbf{x}}$ defined on the domain D , and in the simplest case can describe the accumulation points of minimising sequences $\{u_k\}_{k=1}^\infty$ of functions $u_k : D \rightarrow \mathbb{R}$ in $L_\infty(D)$. Each u_k generates for $\mathbf{x} \in D$ a.e. a linear continuous functional for any continuous function $\varphi \in C_{00}(\mathbb{R})$ with compact support: $\varphi \mapsto \varphi(u_k(\mathbf{x})) = \langle \delta_{u_k(\mathbf{x})}, \varphi \rangle =: \langle \nu_{\mathbf{x}}^{(u_k)}, \varphi \rangle$, i.e. the probability measure $\nu_{\mathbf{x}}^{(u_k)} := \delta_{u_k(\mathbf{x})}$. The YMs arise when the sequence $\{u_k\}$ is bounded in L_∞ (and hence the $\{\nu_{\mathbf{x}}^{(u_k)}\} = \{\delta_{u_k(\mathbf{x})}\}$ are “tight”), as then there is a weak* convergent sub-sequence (for the sake of simplicity with unchanged indices) $u_k \xrightarrow{*} u$, such that the sequence $\{\varphi(u_k)\}$ also converges weak*.

The weak*-limit

$$\varphi(u_k) = \left[\mathbf{x} \mapsto \langle \nu_{\mathbf{x}}^{(u_k)}, \varphi \rangle \right] \xrightarrow{*} \left[\mathbf{x} \mapsto \int_{\mathbb{R}} \varphi(\mathbf{y}) \nu_{\mathbf{x}}^{(u)}(d\mathbf{y}) =: \langle \nu_{\mathbf{x}}^{(u)}, \varphi \rangle =: \varphi_u(\mathbf{x}) \right] \in L_\infty(D)$$

defines again a linear continuous functional and hence the YM $\nu_{\mathbf{x}}^{(u)}$ (the “narrow” limit of the $\{\nu_{\mathbf{x}}^{(u_k)}\} = \{\delta_{u_k(\mathbf{x})}\}$), a measurable system of parametrised probability measures.

As the point-wise accumulation points of $\{\varphi(u_k(\mathbf{x}))\}$ may be different from $\varphi(u(\mathbf{x}))$, this may be overcome with the YM generated by the sequence, which describes the limit as $\varphi_u(\mathbf{x}) = \langle \nu_{\mathbf{x}}^{(u)}, \varphi \rangle$, which may be seen as the expected value of φ w.r.t. the probability measure $\nu_{\mathbf{x}}^{(u)}$.

YM have limitations to describe fracture and damage fields. The YM corresponding to a damage (or fracture) field, may describe the probability distribution $\nu_{\mathbf{x}}$ of the damage at a particular point \mathbf{x} . However, information about spatial correlations is lacking in such a setting. Particularly, probabilities that the crack appears in a point \mathbf{y} conditional on a crack at another point \mathbf{x} cannot be described.

These limitations can be overcome with RFs as “stochastic solutions”. If we have a RF $\mathbf{a} \in \mathcal{P} = \mathcal{S} \otimes \mathcal{P} = L_2(\Theta) \otimes H^1(D) \cong L_2(\Theta; H^1(D))$, similarly as before for any $\varphi \in C_{00}(\mathbb{R})$ one has that for $\mathbf{x} \in D$ a.e. the expression $\mathbb{E}[\varphi \circ \mathbf{a}(\cdot, \mathbf{x})] = \mathbb{E}[\varphi(\mathbf{a}(\cdot, \mathbf{x}))]$ is a

linear continuous functional of φ , and thus defines a probability measure (a YM) $\nu_{\mathbf{x}}^{(\mathbf{a})}$ with the same properties as before.

It is the distribution of the RV $\mathbf{a}(\cdot, \mathbf{x})$, and if the “stochastic solution” is deterministic, i.e. the RF $\theta \mapsto \mathbf{a}(\theta, \mathbf{x}) = \alpha(\mathbf{x})$ is constant, then $\nu_{\mathbf{x}}^{(\mathbf{a})} = \delta_{\alpha(\mathbf{x})}$. But a RF \mathbf{a} can also describe all desired kinds of n -point correlation measures $\langle \nu_{\mathbf{x}_1, \dots, \mathbf{x}_n}^{(\mathbf{a})}, \varphi \rangle = \mathbb{E}[\varphi \circ (\prod_{i=1}^n \mathbf{a}(\cdot, \mathbf{x}_i))]$ for $\mathbf{x}_1, \dots, \mathbf{x}_n \in D$, and is thus much more informative than a YM, hence the “stochastic solutions” here have at least the same descriptive power as the “statistical solutions” in [42, 38], which are characterized by such families of correlation measures.

4.4 Numerical computations

Section 4.2 has outlined a stochastic reformulation of variational problems. In this section, we will introduce sampling approximations for numerical computations and illustrate the procedure with the anti-plane shear test case. Before proceeding, we summarize our strategy to obtain the QoIs as follows:

- (i) perturbation of the parameters \mathbf{q} of the problem by a zero-mean RV $\tilde{\mathbf{q}} : \Theta \rightarrow \mathcal{Q}$ (e.g. $\tilde{\mathbf{q}} \in L_2(\Theta; \mathcal{Q})$) and a positive parameter η , i.e. the parameters of the problem are considered as

$$\mathbf{q}_\eta(\theta) = q_0 + \eta \tilde{\mathbf{q}}(\theta). \quad (31)$$

- (ii) Use of a (numerical) solver to obtain a realization of the output RV $\mathcal{Y}_\eta(\mathbf{u}(\theta), \mathbf{a}(\theta))$.
- (iii) Numerical computation of the QoIs $\mathbb{E}[\mathcal{Y}_\eta(\mathbf{u}, \mathbf{a})]$, e.g. mean value or variance, through a sampling method.

Note that the variational problems may have multiple solutions, but a numerical solver provides a unique solution for each parameter. This allows us to make use of RVs in the usual way. Thanks to the perturbation, the resulting algorithm still provides a RV. Yet, the influence of the solver on the numerical algorithm and results remains questionable. Note also that the solution operator may be discontinuous as a small change in the parameters may lead to a significantly different response. This makes the functional approximation of the solution operator complicated and an approximation, which allows to describe discontinuities, is required. In this sense, the Monte Carlo method is a sensible choice.

The theoretical results of the previous section will now be illustrated returning to the anti-plane shear test. Following the approach outlined so far we first introduce the random perturbations before applying the Monte Carlo algorithm.

4.4.1 Random perturbations

In this case, among many possible stochastic inputs, we focus on a probabilistic modeling of the geometry. Note that a stochastic geometry is typically handled by transforming back the perturbed domain to a deterministic reference domain and the weak formulation is

expressed on this reference domain using pull-back operators. After applying the pull-back, only the material tensors are random. Hence, a random geometry setting is closely related to Section 4.2, where a perturbation of the material parameter on a fixed domain was considered for illustration purposes. In the context of the mechanical problem considered here, it is expected that the shape of the hole will have a significant influence on the formation of the crack path.

Therefore, we perturb the hole geometry using a rather general approach for star-shaped objects, which is employed in inverse problems and uncertainty studies, see [37] for instance. Particularly, the hole geometry $\{\mathbf{x}(r, \varphi) = (r \cos \varphi, r \sin \varphi) \mid \text{for } r = R > 0 \text{ and } \varphi \in [0, 2\pi)\}$ expressed in polar coordinates is randomised by perturbing its radius

$$\mathbf{q}_\eta(\theta) = R + \eta \tilde{\mathbf{q}}(\theta) \quad \text{with} \quad \tilde{\mathbf{q}}(\theta) = \sum_{j=1}^J c_j y_{2j-1}(\theta) \cos(j\varphi) + s_j y_{2j}(\theta) \sin(j\varphi), \quad (32)$$

where R refers to the unperturbed (nominal) radius of a circle, η controls the magnitude of the perturbation and c_j, s_j are deterministic coefficients which are used to weight the influence of the different harmonics. In particular we set $c_j = s_j = \frac{1}{j}$ such that the influence of higher harmonics is successively decreasing. Finally, in (32), $y_k : \Theta \rightarrow \mathbb{R}, k = 1, \dots, 2J$ are assumed to be uniformly distributed RVs on the interval $[-1, 1]$. We additionally assume that the RVs are independent of each other. The parameterization introduced through $y_i, i = 1, \dots, 2J$ enables the generation of RF samples by simply drawing uniformly distributed pseudo-random numbers. It should be further noted that (32) represents a Karhunen-Loève expansion, introduced in Section 4.2, which is more commonly known as proper orthogonal decomposition in the context of reduced order modeling. Note that we now use the Karhunen-Loève expansion for the input data.

In a specific application scenario, (32) can be used to model uncertainties in the geometry due to manufacturing imperfections. Measurement data, based on imaging for instance, could then be used to infer the probability distribution of the coefficients c_j and s_j and possible correlations. These aspects are, however, not elaborated in any detail here.

4.4.2 Computing statistical moments

We employ the Monte Carlo method based on a sample $\{\mathbf{q}_\eta^{(i)}\}_{i=1}^M$ of the perturbed parameter. Such a sample can be obtained with separated representations, the Karhunen-Loève expansion in particular, which has already been introduced in Section 4.2 and will be illustrated below through a specific example. We then employ a numerical solver to obtain $\mathbf{Y}_{\eta,h}(\mathbf{u}^{(i)}, \mathbf{a}^{(i)})$, where h denotes a discretization parameter. This allows to approximate QoIs, e.g.

$$\begin{aligned} \mu &:= \mathbb{E}[\mathbf{Y}_{\eta,h}(\mathbf{u}, \mathbf{a})] \approx \frac{1}{M} \sum_{i=1}^M \mathbf{Y}_{\eta,h}(\mathbf{u}^{(i)}, \mathbf{a}^{(i)}) =: \mu_{\eta,h}, \\ \text{var}_{\mathbf{Y}_{\eta,h}(\mathbf{u}, \mathbf{a})} &\approx \frac{1}{M} \sum_{i=1}^M (\mathbf{Y}_{\eta,h}(\mathbf{u}^{(i)}, \mathbf{a}^{(i)}) - \mu_{\eta,h})^2. \end{aligned}$$

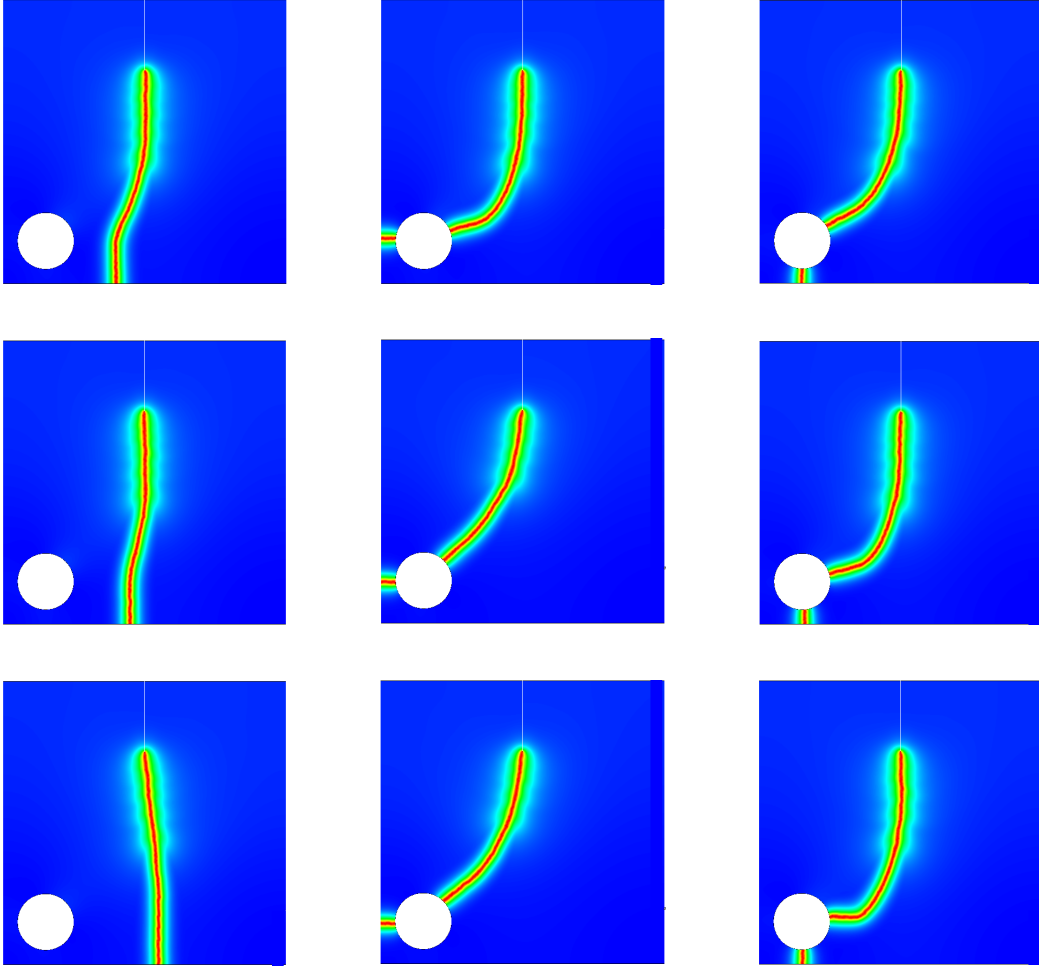


Figure 12: Different realizations of the Monte Carlo simulation. All three characteristic crack patterns from the deterministic simulations appear, see Table 3.

We now report the stochastic numerical results for our anti-plane shear test. This subsection focuses on the mean value and variance of the phase field, whereas computing crack pattern probabilities is treated in the next subsection. We employ Mesh 2 with $(h_{\min}, h_{\max}) = (\frac{1}{4}\ell, \ell)$ and the radius of the hole given by (32). The applied displacement is given by $\bar{\mathbf{u}}_n = n\Delta\bar{\mathbf{u}}$, $n = 1, \dots, 15$ with $\Delta\bar{\mathbf{u}} = 0.1$. Results shown (final crack pattern) will be those of the last loading step.

Figure 12 depicts the crack phase field solution $\alpha^{(i)}$ at nine different realizations $i_1, i_2, \dots, i_9 \in \{1, \dots, M\}$. These realizations illustrate the strong variability of the crack pattern which is triggered by randomly perturbing the geometry. Note that all three crack patterns obtained in the deterministic simulations of Section 2 by perturbing the finite element mesh and classified in Table 3 are re-obtained here. However, crack types 2 and 3 show little deviations in different realizations, whereas crack type 1 covers a wider range of geometries, the final portion of the crack being located within a band close to the center of the specimen.

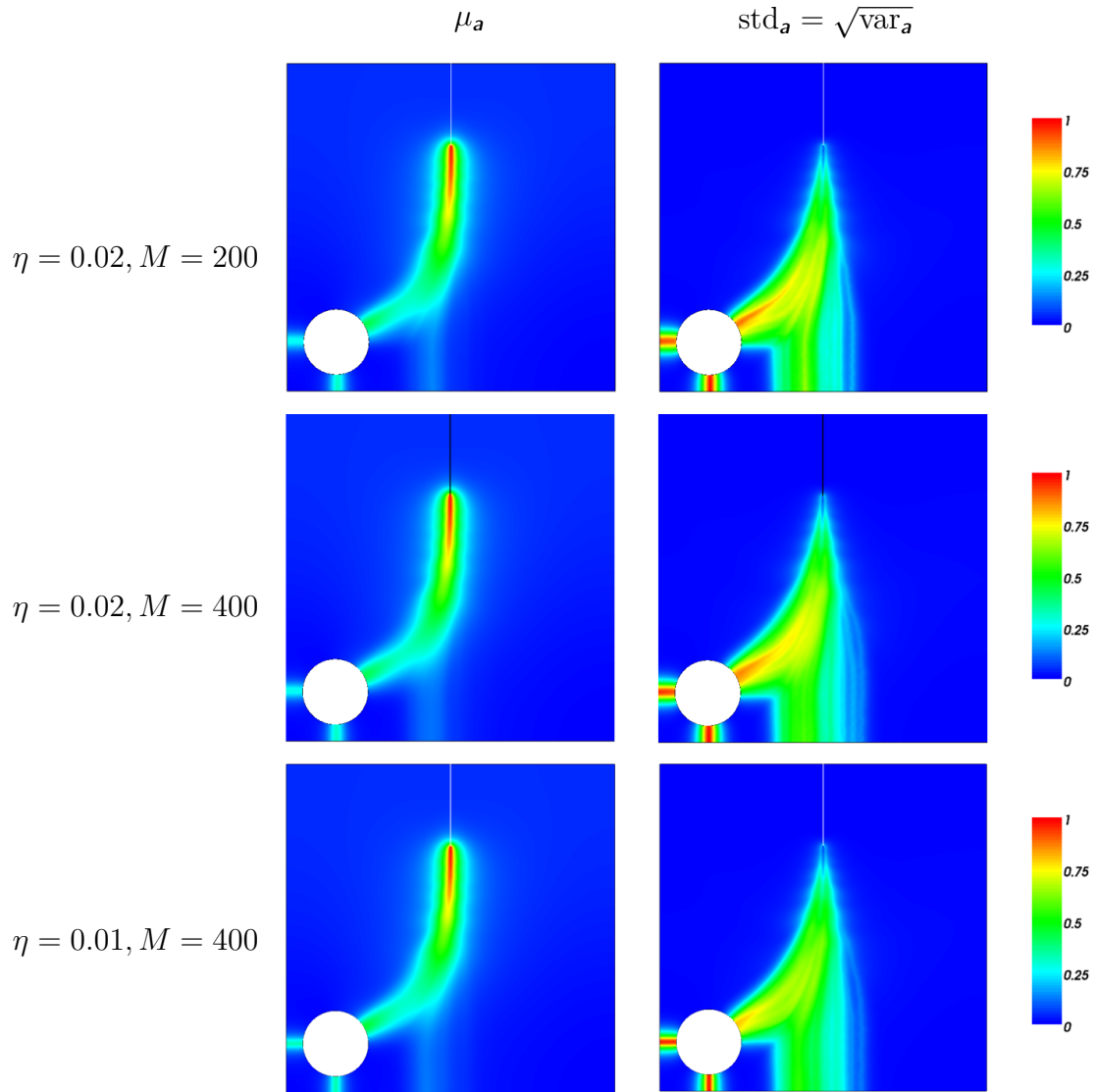


Figure 13: Expected value μ_a and standard deviation $\text{std}_a = \sqrt{\text{var}_a}$ of the phase field for different magnitudes of η and M .

In Figure 13 (top) we plot the estimated expected value and the standard deviation of the phase field for a perturbation amplitude of $\eta = 0.02$ and a sample size $M = 200$. Clearly, both the expected value and the standard deviation feature all three crack patterns observed already in Figure 12. The expected value of the phase field is particularly high directly at the notch where each crack begins. Among the three observed paths, the lowest values are obtained along the crack pattern remote from the hole (Type 1), which can be explained by the stronger spatial scattering in this area causing a smearing out of the phase field mean value. Conversely, the larger amplitudes for Type 2,3 cracks are attributed to

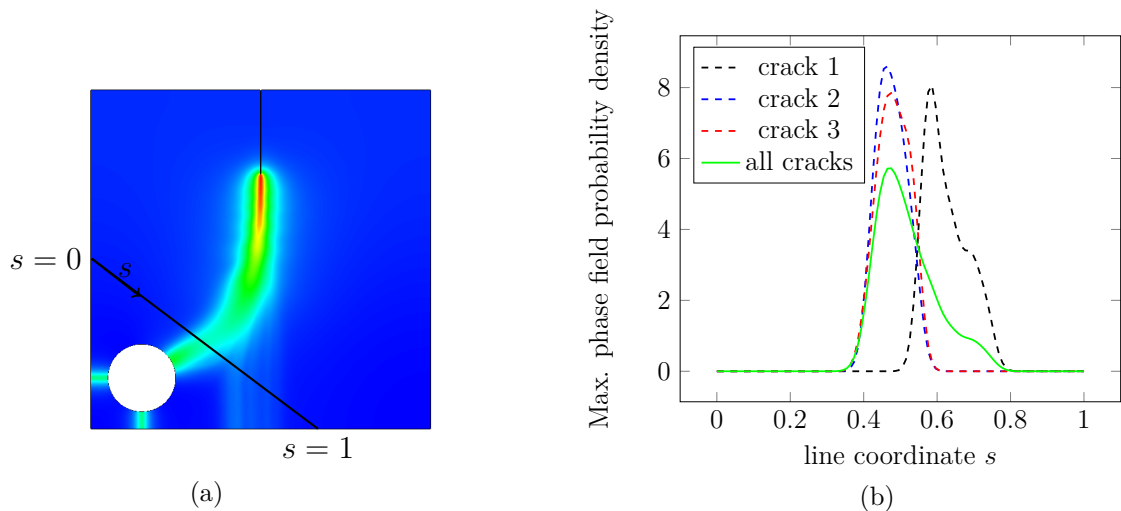


Figure 14: (a) Mean value of the phase field variable for $\eta = 0.0025$ and $M = 200$. Indicated is also the line $y = -\frac{2}{3}x + 1$ within the domain $D = [0, 2] \times [0, 2]$ with coordinate s , and (b) Probability density functions of the maximum phase field value along coordinate s for all crack types.

the localization of the paths along the holes. Also the standard deviation is observed to be more concentrated for crack patterns passing through the hole (Type 2 and 3), whereas the band appearing in the center of the specimen for the Type 1 crack confirms the larger variability of this crack path. Figure 13 (middle) contains the same quantities with an increased sample size of $M = 400$. Visually there is not much difference between the two plots. Increasing the sample size seems to lead to a more homogeneous mean and variance crack field along the vertical line in the middle of the domain.

For the largest sample size, i.e. $M = 400$, we report the same numerical results, however, for a different perturbation magnitude $\eta = 0.01$ in Figure 13 (bottom). The crack distributions largely resemble those obtained with $\eta = 0.02$. Differences can be identified in particular for the variance in the vicinity of the hole, yet this may represent a statistical effect, in view of the given sample size. Results for even smaller perturbation sizes (up to a minimum tested value of $\eta = 0.0025$) are not reported, since they show a qualitatively similar behavior.

4.4.3 Computing crack pattern probabilities

We recall that three different crack types occur for this application, referred to as crack 1, 2, 3 see Table 3. To compute the corresponding probabilities of occurrence, the range of the phase field random variable $\mathbf{a}(\theta)$ is clustered into three disjoint domains, i.e. $\mathbf{a}(\Theta) \in \bigcup_{i=1}^3 C_i \subset \mathcal{P}_n$, corresponding to the three cracks, where n represents the final loading step. Then, the probabilities $\mathbb{P}(\mathbf{a} \in C_i) = \mathbb{E}[\mathbb{1}_{C_i} \circ \mathbf{a}]$ for $i = 1, 2, 3$ are numerically approximated

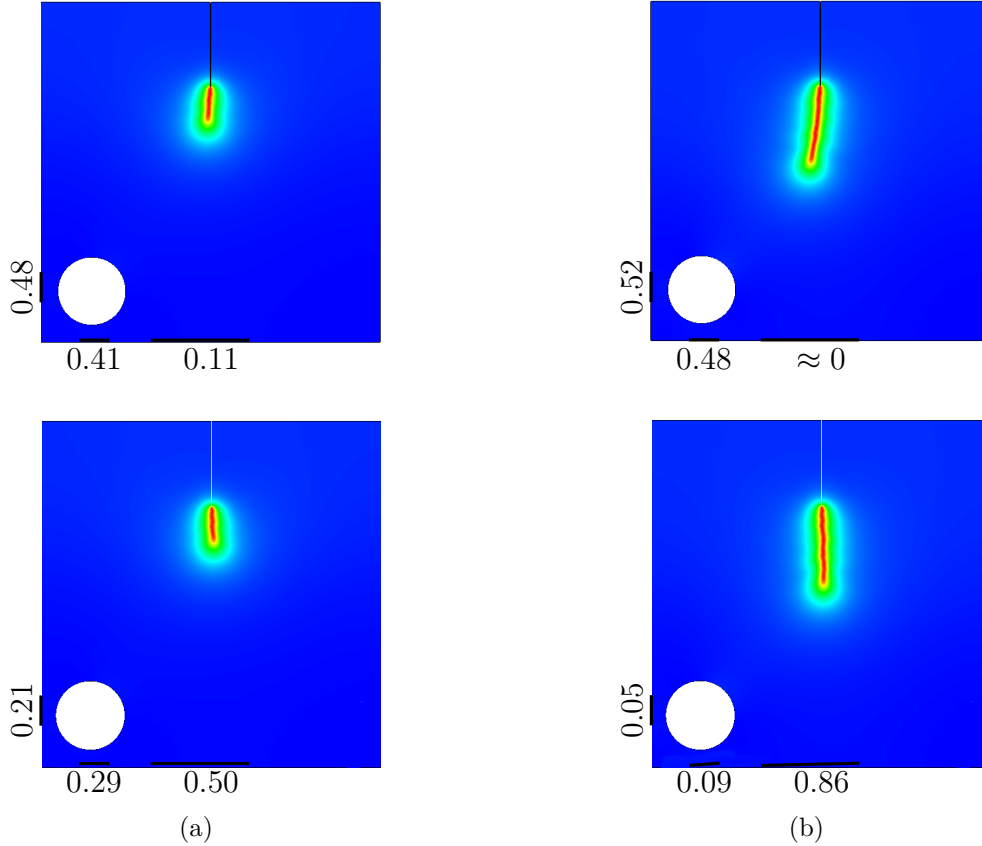


Figure 15: Particular realizations of phase field variables at two different loading steps for $\eta = 0.0025$ and $M = 200$. The numbers refer to computed conditional crack probabilities for each different crack type, based on a Monte Carlo sample. (a) Cracks at loading step $n = 9$ and (b) cracks at loading step $n = 11$.

with a sample as $p_i = \frac{1}{M} \sum_{m=1}^M \mathbb{1}_{C_i} \circ \mathbf{a}^{(m)}$. For a perturbation magnitude of $\eta = 0.01$ and $M = 200$, we obtain $p_1 = 0.325$, $p_2 = 0.335$, and $p_3 = 0.340$. Hence, the probabilities seem to be comparable, of approximately $1/3$, for each crack type. These numbers do not change significantly when the perturbation is varied. For instance, if $\eta = 0.02$ and $M = 200$, we obtain $p_1 = 0.3$, $p_2 = 0.33$, and $p_3 = 0.37$.

We proceed by discussing the possibility of updating probabilities during crack propagation. This could be useful to analyze and assess initiated but not fully developed cracks. To this end, conditioning on a given damage state is required. We simplify the computations by considering a cut of the domain, see Figure 14 on the left.

We assume that all cracks pass through a line $L = \{\mathbf{x} \in D \mid \mathbf{x} = \mathbf{p} + s\mathbf{u}, s \in [0, 1]\}$, which is represented by a RV $y : \Theta \rightarrow L$ defined as $y(\theta) = \arg \max_{\mathbf{x} \in L} \{\mathbf{a}_n(\theta, \mathbf{x}) \mid, n \geq 1\}$. The probability of a particular intersection point of the crack with the line is characterised with the probability density $f_y : L \rightarrow [0, \infty)$. Here, we approximate the density with kernel estimation based on the sample $\{y^{(i)}\}_{i=1}^M$, see Figure 14. Moreover, based on the

partitioning of the range of \mathbf{a} , we can also estimate the conditional probability densities $f_{y|C_i}$ for individual cracks. We observe that the conditional densities for cracks 2, 3 nearly coincide, which is expected, since the domain is cut before the cracks reach the hole where it is almost impossible to distinguish between both crack patterns.

Next, we address the computation of conditional probabilities, i.e. the probability that crack C_1 happens when the intersection of the crack with a line L is observed at a position x_c . Mathematically, this computation builds on Bayes' theorem

$$\mathbb{P}(\mathbf{a} \in C_1 | y = x_c) = \frac{f_{y|C_1}(x_c)\mathbb{P}(\mathbf{a} \in C_1)}{f_y(x_c)}, \quad (33)$$

where $\mathbb{P}(\mathbf{a} \in C_1) = p_1$ is the total probability that crack C_1 occurs, $f_y(x_c)$ is the probability of the crack at point x_c (obtained from the green line in Figure 14), and $f_{y|C_1}(x_c)$ is the conditional probability of a crack intersecting at x_c for a crack of type C_1 (obtained from the dashed black line in Figure 14). Figure 15 shows cracks at different stages of their evolution, together with the associated crack type probabilities. The upper plots depict a crack through the hole for $n = 9$ and $n = 11$, respectively. Already after bending slightly to the left (upper left plot) the probability of obtaining a type 1 crack, not passing through the hole, is significantly reduced. After two additional loading steps (upper right plot) the associated probability is almost zero. The two plots on the bottom represent a type 1 crack, again at loading stages $n = 9$ and $n = 11$, respectively. This crack initially is slightly deviated to the right, which causes the type 1 probability to increase. At loading step $n = 11$ (bottom right plot) the probability of passing through the hole is already very low. These examples show the large influence of conditioning the crack probabilities to partially developed crack patterns. We emphasize that these computations critically rely on correlation information for the phase field at different points in the computational domain. Such information is naturally available in the stochastic solution setting of the paper.

5 Conclusions

The phase field approach can cope with several challenges in the computational treatment of brittle fracture. However, its solution is non-unique in general, and this raises the question of the meaning and representativeness of the (possibly several) solutions which can be found numerically. Through an illustrative test case we have exposed the non-uniqueness of the solution due to competing energy levels of a variety of crack paths. In particular, the crack propagation was found to be highly sensitive to meshing and geometric perturbations. No other types of perturbations were tested.

In view of these findings, we have introduced the concept of a ‘‘stochastic solution’’ in the form of random fields as a new and general concept in brittle fracture, allowing one to obtain various crack patterns and their probabilities.

Random fields can capture correlations, which is not possible with standard Young measures for instance. They further permit to condition on not fully developed crack paths,

which is interesting from a practical perspective. The stochastic solution concept does not remove the problem of non-uniqueness in general: one may obtain all possible crack patterns at once, but with possibly non-unique probabilities (see e.g. the example in Section 3.1). However, the computed probabilities in some numerical experiments were comparable, despite the adoption of different solution approaches (see the global minimization for the sharp crack model in Section 3.2 and the local minimization with the regularized model in Section 3.3). Moreover, further numerical tests (not reported in the paper) seem to indicate that, when inducing the geometrical perturbation adopted in Section 4.4, the sensitivity of the stochastic solution, expressed in terms of probability distribution of the different crack paths, with respect to changes in the numerical setup of the problem is lower than the sensitivity of the deterministic solution to such changes. Importantly, the numerical results further showed a dependence of the computed crack probabilities on the type of perturbation (see the three examples in Section 3.2), which is to be expected and also desired from a physical perspective. In general we conjecture the existence of a unique stochastic solution for a given physical perturbation and a formulation providing this unique solution is still to be developed.

References

- [1] G.A. Francfort and J.-J. Marigo. Revisiting brittle fractures as an energy minimization problem. *Journal of the Mechanics and Physics of Solids*, 46:1319–1342, 1998.
- [2] B. Bourdin, G.A. Francfort, and J.-J. Marigo. Numerical experiments in revisited brittle fracture. *Journal of the Mechanics and Physics of Solids*, 48(4):797–826, 2000.
- [3] B. Bourdin. Numerical implementation of the variational formulation for quasi-static brittle fracture. *Interfaces and Free Boundaries*, 9:411–430, 2007.
- [4] B. Bourdin. The variational formulation of brittle fracture: numerical implementation and extensions. In R. de B. A. Combescure T. Belytschko (ed.), *IUTAM Symposium on Discretization Methods for Evolving Discontinuities* (pp. 381–393). Springer, 2007.
- [5] B. Bourdin, G.A. Francfort, and J.-J. Marigo. The variational approach to fracture. *Journal of Elasticity*, 91(1-3):5–148, 2008.
- [6] G. Del Piero, G. Lancioni, and R. March. A variational model for fracture mechanics: numerical experiments. *J. Mech. Phys. Solids*, 55:2513–2537, 2007.
- [7] G. Lancioni and G. Royer-Carfagni. The variational approach to fracture mechanics: A practical application to the French Panthéon in Paris. *J. Elasticity*, 95:1–30, 2009.
- [8] H. Amor, J.-J. Marigo, and C. Maurini. Regularized formulation of the variational brittle fracture with unilateral contact: Numerical experiments. *J. Mech. Phys. Solids*, 57:1209–1229, 2009.
- [9] F. Freddi and G. Royer-Carfagni. Regularized variational theories of fracture: A unified approach. *J. Mech. Phys. Solids*, 58:1154–1174, 2010.
- [10] C. Kuhn and R. Müller. A continuum phase field model for fracture. *Eng. Fracture Mech*, 77:3625–3634, 2010.
- [11] C. Miehe, F. Welschinger, and M. Hofacker. Thermodynamically consistent phase-field models of fracture: variational principles and multi-field FE implementations. *Int. J. Numer. Methods Engrg.*, 83:1273–1311, 2010.
- [12] C. Miehe, M. Hofacker, and F. Welschinger. A phase field model for rate-independent crack propagation: robust algorithmic implementation based on operator splits. *Comput. Methods Appl. Mech. Engrg.*, 199:2765–2778, 2010.
- [13] K. Pham, H. Amor, J.-J. Marigo, and C. Maurini. Gradient damage models and their use to approximate brittle fracture. *Int. J. Damage Mech*, 20(4):618–652, 2011.
- [14] M.J. Borden, T.J.R. Hughes, C.M. Landis, and C.V. Verhoosel. A higher-order phase-field model for brittle fracture: formulation and analysis within the isogeometric analysis framework. *Comput. Methods Appl. Mech. Engrg.*, 273:100–118, 2014.

- [15] J. Vignollet, S. May, R. de Borst, and C.V. Verhoosel. Phase-field models for brittle and cohesive fracture. *Meccanica*, 49:2587–2601, 2014.
- [16] A. Mesgarnejad, B. Bourdin, and M.M. Khonsari. Validation simulations for the variational approach to fracture. *Comput. Methods Appl. Mech. Engr.*, 290:420–437, 2015.
- [17] C. Kuhn, A. Schlüter, and R. Müller. On degradation functions in phase field fracture models. *Comp. Material Science*, 108:374–384, 2015.
- [18] M. Ambati, T. Gerasimov, and L. De Lorenzis. A review on phase-field models of brittle fracture and a new fast hybrid formulation. *Computational Mechanics*, 55(2):383–405, 2015.
- [19] J.-J. Marigo, C. Maurini, and K. Pham. An overview of the modelling of fracture by gradient damage models. *Meccanica*, 51:3107–3128, 2016.
- [20] E. Tanné, T. Li, B. Bourdin, J.-J. Marigo, and C. Maurini. Crack nucleation in variational phase-field models of brittle fracture. *J. Mech. Phys. Solids*, 110:80–99, 2018.
- [21] J.M. Sargado, E. Keilegavlen, I. Berre, and J.M. Nordbotten. High-accuracy phase-field models for brittle fracture based on a new family of degradation functions. *J. Mech. Phys. Solids*, 111:458–489, 2018.
- [22] T. Gerasimov, N. Noii, O. Allix, and L. De Lorenzis. A non-intrusive global/local approach applied to phase-field modeling of brittle fracture. *Adv. Model. and Simul. in Eng. Sci.*, 5:14, 2018.
- [23] J.-Y. Wu, and V.P. Nguyen. A length scale insensitive phase-field damage model for brittle fracture. *J. Mech. Phys. Solids*, 119:20–42, 2018.
- [24] M. Negri, and C. Ortner. Quasi-static crack propagation by Griffith’s criterion. *Math. Mod. Meth. Appl. Sci.*, 18:1895-1925, 2008.
- [25] T. Gerasimov and L. De Lorenzis. A line search assisted monolithic approach for phase-field computing of brittle fracture. *Comput. Methods Appl. Mech. Engrg.*, 312:276–303, 2016.
- [26] T. Wick. An error-oriented Newton/inexact augmented Lagrangian approach for fully monolithic phase-field fracture propagation. *SIAM J. Sci. Comput.*, 39(4):589–6017, 2017.
- [27] S. Burke, C. Ortner, E. Süli. An adaptive finite element approximation of a variational model of brittle fracture. *SIAM J. Numer. Anal.*, 48(3):980–1012, 2010.
- [28] S. Burke, C. Ortner, E. Süli. An adaptive finite element approximation of a generalized Ambrosio-Tortorelli functional. *Math. Models Methods Appl. Sci.*, 23(9):1663—1697, 2013.

- [29] M. Artina, S. Micheletti, S. Perotto, and M. Fornasier. Anisotropic adaptive meshes for brittle fractures: parameter sensitivity. In: Abdulle, A., Deparis, S., Kressner, D., Nobile, F., Picasso, M. (eds.), *Numerical Mathematics and Advanced Applications*, pages 293—302, Springer-Verlag, Berlin Heidelberg, Germany, 2014.
- [30] M. Artina, M. Fornasier, S. Micheletti, and S. Perotto. Anisotropic mesh adaptation for crack detection in brittle materials. *SIAM J. Scientific Computing*, 37(4):633–659, 2015.
- [31] T. Gerasimov and L. De Lorenzis. On penalization in variational phase-field models of brittle fracture. *Comput. Methods Appl. Mech. Engrg.*, 354:990–1026, 2019.
- [32] A. Braides. Approximation of free-discontinuity problems, in: *Lecture Notes in Mathematics*, Springer-Verlag, 1998.
- [33] A. Chambolle. An approximation result for special functions with bounded deformation. *J. Math. Pures Appl.* 83, 929–954, 2004.
- [34] L. Ambrosio, V.M. Tortorelli. Approximation of functional depending on jumps by elliptic functional via Gamma-convergence. *Commun. Pure Appl. Math.*, 43(8):999–1036, 1990.
- [35] F. Hecht, A. Leharic, and O. Pironneau. FreeFem++: Language for finite element method and Partial Differential Equations (PDE), Université Pierre et Marie, Laboratoire Jacques-Louis Lions, <http://www.freefem.org/ff++/>.
- [36] A.R. Ingraffea, and M. Grigoriu. Probabilistic fracture mechanics: a validation of predictive capability. Technical report, DTIC Document, 1990.
- [37] R. Hiptmair, L. Scarabosio, C. Schillings, and C. Schwab. Large deformation shape uncertainty quantification in acoustic scattering, *Advances in Computational Mathematics*, 44(5):1475–1518, 2018.
- [38] U. Fjordholm, S. Mishra, and E. Tadmor. On the computation of measure-valued solutions, *Acta Numerica*, 25: 567–679, 2016.
- [39] U. Fjordholm, R. Käppeli, S. Mishra, and E. Tadmor. Construction of approximate entropy measure-valued solutions for hyperbolic systems of conservation laws, *Foundations of computational mathematics*, 17(3): 763–827, 2017.
- [40] S. Lanthaler, and S. Mishra. Computation of measure-valued solutions for the incompressible Euler equations, *Mathematical Models and Methods in Applied Sciences*, 25(11): 2043–2088, 2015.
- [41] U. S. Fjordholm, K. Lye, and S. Mishra. Numerical Approximation of Statistical Solutions of Scalar Conservation Laws. *SIAM Journal on Numerical Analysis*, 56(5):2989–3009, 2018.

- [42] U. S. Fjordholm, S. Lanthaler, and S. Mishra. Statistical Solutions of Hyperbolic Conservation Laws: Foundations. *Archive for Rational Mechanics and Analysis*, 226(2):809–849, 2017.
- [43] T. Roubíček. *Relaxation in Optimization Theory and Variational Calculus*. Walter de Gruyter, Berlin, New York, 1997.
- [44] P. Pedregal. *Parameterized measures and variational principles*. Birkhäuser, Basel, 1997.
- [45] B. Benesova, and M. Kružík. Weak Lower Semicontinuity of Integral Functionals and Applications. *SIAM Review*, 59(4):703–766, 2017.
- [46] M. Kružík, and A. Prohl. Young measure approximation in micromagnetics. *Numerische Mathematik*, 90(2):291–307, 2001.
- [47] M. Kružík, A. Mielke, and T. Roubíček. Modelling of Microstructure and its Evolution in Shape-Memory-Alloy Single-Crystals, in Particular in CuAlNi. *Meccanica*, 40(4-6):389–418, 2005.
- [48] D. Henrion, M. Kružík, and T. Weisser. Optimal control problems with oscillations, concentrations and discontinuities. *Automatica*, 103:159–165, 2019.
- [49] M. Kružík, and T. Roubíček. Optimization Problems With Concentration And Oscillation Effects: Relaxation Theory And Numerical Approximation. *Numerical Functional Analysis and Optimization*, 20(5-6):511–530, 1999.
- [50] R. J. DiPerna, and A. J. Majda. Oscillations and concentrations in weak solutions of the incompressible fluid equations. *Communications in Mathematical Physics*, 108(4):667–689, 1987.
- [51] J. M. Hammersley, and D. C. Handscomb. *Monte Carlo Methods*, Methuen and Co. Ltd., London, 1964.
- [52] M. Loève. *Probability Theory I*, Springer, Berlin, 1977.
- [53] M. Loève. *Probability Theory II*, Springer, Berlin, 1978.
- [54] R. G. Ghanem, P. D. Spanos, *Stochastic Finite Elements: A Spectral Approach*, Springer, Berlin, 1991.
- [55] H. G. Matthies, Chr. Bucher: *Finite elements for stochastic media problems*. *Computer Methods in Applied Mechanics and Engineering* **168** (1999) 3–17. doi:10.1016/S0045-7825(98)00100-5.
- [56] I. Babuška, R. Tempone, and G. E. Zouraris. Galerkin finite element approximations of stochastic elliptic partial differential equations. *SIAM Journal on Numerical Analysis*, 42(2): 800–825, 2004.

- [57] H. G. Matthies, A. Keese. Galerkin methods for linear and nonlinear elliptic stochastic partial differential equations, *Computer Methods in Applied Mechanics and Engineering*, **194**(12–16): 1295–1331, 2005. doi:10.1016/j.cma.2004.05.027.
- [58] H. G. Matthies, B. Rosić: *Inelastic Media under Uncertainty: Stochastic Models and Computational Approaches*. In: B. D. Reddy (ed.): *IUTAM Symposium on Theoretical, Computational, and Modelling Aspects of Inelastic Media*, pp. 185–195, IUTAM Book-series Vol. 11. Springer-Verlag, Berlin, 2008. doi:10.1007/978-1-4020-9090-5_17.
- [59] B. V. Rosić, H. G. Matthies: *Stochastic Galerkin Method for the Elastoplasticity Problem*. In: D. Müller-Hoppe, S. Löhner, and S. Reese (eds.): *Recent Developments and Innovative Applications in Computational Mechanics*. pp. 303–310, Springer-Verlag, Berlin, 2011. doi:10.1007/978-3-642-17484-1_34.
- [60] B. V. Rosić, H. G. Matthies: *Variational Theory and Computations in Stochastic Plasticity*. *Archives of Computational Methods in Engineering* **22** (2015) 457–509. doi:10.1007/s11831-014-9116-x.
- [61] T. J. Sullivan. *Introduction to Uncertainty Quantification*, Texts in Applied Mathematics Vol. 63, Springer, Berlin, 2015. doi:10.1007/978-3-319-23395-6.
- [62] P. A. Besold, *Solutions to Stochastic Partial Differential Equations as Elements of Tensor Product Spaces*, PhD thesis, Mathematica Gottingensis, Universität Göttingen, 2000. url:\protect\vrulewidth0pt\protect\href{http://webdoc.sub.gwdg.de/ebook/e/2000/mathe-goe/Pbesold3.pdf}{http://webdoc.sub.gwdg.de/ebook/e/2000/mathe-goe/Pbesold3.pdf}.
- [63] H. G. Matthies, R. Ohayon: *Analysis of parametric models — linear methods and approximations*. *Advances in Computational Mathematics* **45** (2019) 2555–2586. doi:10.1007/s10444-019-09735-4.
- [64] K. Karhunen, *Über lineare Methoden in der Wahrscheinlichkeitsrechnung*. *Ann. Acad. Sci. Fennicae. Ser. A. I. Math.-Phys.*, **37** (1947) 1–79. English translation: url:https://www.rand.org/pubs/translations/T131.html.
- [65] M. Kružík, and T. Roubíček. *Mathematical methods in continuum mechanics of solids*. Springer, Berlin, 2019.
- [66] A. Mielke, and T. Roubíček. *Rate-independent systems: theory and application*. Applied mathematical sciences. Springer, Berlin, 2015.
- [67] S. N. Armstrong, and Z. Shen. Lipschitz estimates in almost-periodic homogenization. *Communications on pure and applied mathematics*, 69(10): 1882–1923, 2016.
- [68] X. Li, J. Shi, X. Dong, and J. Yu. A new conjugate gradient method based on Quasi-Newton equation for unconstrained optimization. *Journal of computational and applied mathematics*, 2018.

- [69] G. Francfort, and J.-J. Marigo. Cracks in fracture mechanics: a time indexed family of energy minimizers. In IUTAM Symposium on variations of domain and free-boundary problems in solid mechanics, pp. 197–202. Springer, Dordrecht, 1999.
- [70] M. Jirásek, J. Zeman, and J. Vondřejc. Softening gradient plasticity: analytical study of localization under nonuniform stress. *International journal for multiscale computational engineering*, 8(1): 37–60, 2010.
- [71] O. Rokoš, J. Zeman, and M. Jirásek. Localization analysis of an energy-based fourth-order gradient plasticity model. *European journal of mechanics - A/Solids*, 55: 256–277, 2016.
- [72] M. Jirásek, and J. Zeman. Localization study of a regularized damage model. *International journal of solids and structures*, 69-70: 131–151, 2015.
- [73] M. Jirásek, O. Rokoš, and J. Zeman. Localization analysis of variationally based gradient plasticity model. *International journal of solids and structures*, 50(1): 256–269, 2013.
- [74] A. Fiaschi, D. Knees, and U. Stefanelli. Young-Measure Quasi-Static Damage Evolution. *Arch. Rational Mech. Anal.* **203** (2012) 415–453. doi:10.1007/s00205-011-0474-3.
- [75] C. Foiaş, O. Manley, R. Rosa, and R. Temam. Navier–Stokes Equations and Turbulence. *Encyclopedia of Mathematics and its Applications*, **83**. Cambridge University Press, Cambridge, 2004.
- [76] I. E. Segal. Tensor algebras over Hilbert spaces I. *Transactions of the American Mathematical Society* **81** (1956), no. 1, 106–134. doi:10.2307/1993234.
- [77] I. E. Segal. Distributions in Hilbert space and canonical systems of operators. *Transactions of the American Mathematical Society* **88** (1958), no. 1, 12–41. doi:10.2307/1993234.
- [78] I. E. Segal. Nonlinear functions of weak processes. I. *Journal of Functional Analysis* **4** (1969), no. 3, 404–456. doi:10.1016/0022-1236(69)90007-X.
- [79] I. M. Gel’fand and N. Y. Vilenkin. Applications of harmonic analysis, *Generalized Functions*, vol. 4, Academic Press, New York, NY, 1964.
- [80] K. Marti. *Stochastic Optimixation Methods*. Springer, Berlin, 2005.
- [81] A. K. Tyagi, et al. Hybrid importance sampling Monte Carlo approach for yield estimation in circuit design. *Journal of Mathematics in Industry* **8.1** (2018), 11.